EUROPEAN ORGANIZATION FOR NUCLEAR RESEARCH

Prompt D^0, D^+, and D^{*+} production in Pb–Pb collisions at $\sqrt{s_{NN}} = 5.02$ TeV

ALICE Collaboration*

Abstract

The production of prompt D^0, D^+, and D^{*+} mesons was measured at midrapidity ($|y| < 0.5$) in Pb–Pb collisions at the centre-of-mass energy per nucleon–nucleon pair $\sqrt{s_{NN}} = 5.02$ TeV with the ALICE detector at the LHC. The D mesons were reconstructed via their hadronic decay channels and their production yields were measured in central (0–10%) and semicentral (30–50%) collisions. The measurement was performed up to a transverse momentum (p_T) of 36 or 50 GeV/c depending on the D meson species and the centrality interval. For the first time in Pb–Pb collisions at the LHC, the yield of D^0 mesons was measured down to $p_T = 0$, which allowed a model-independent determination of the p_T-integrated yield per unit of rapidity (dN/dy). A maximum suppression by a factor 5 and 2.5 was observed with the nuclear modification factor (R_{AA}) of prompt D mesons at $p_T = 6$–8 GeV/c for the 0–10% and 30–50% centrality classes, respectively. The D-meson R_{AA} is compared with that of charged pions, charged hadrons, and J/ψ mesons as well as with theoretical predictions. The analysis of the agreement between the measured R_{AA}, elliptic (v_2) and triangular (v_3) flow, and the model predictions allowed us to constrain the charm spatial diffusion coefficient D_s. Furthermore the comparison of R_{AA} and v_2 with different implementations of the same models provides an important insight into the role of radiative energy loss as well as charm quark recombination in the hadronisation mechanisms.

---

*See Appendix A for the list of collaboration members

arXiv:2110.09420v1 [nucl-ex] 18 Oct 2021

1 Introduction

Ultra-relativistic heavy-ion collisions allow the study of quantum chromodynamics (QCD) at high energy density and temperature. According to lattice QCD (lQCD) calculations, these extreme conditions lead to a transition of hadronic matter into a strongly-interacting medium, called quark–gluon plasma (QGP), in which quarks and gluons are deconfined and chiral symmetry is partially restored [1–5]. A QGP is formed and studied in high-energy heavy-ion collisions at the Relativistic Heavy Ion Collider (RHIC) and at the CERN Large Hadron Collider (LHC). The existing measurements indicate that the QGP behaves as a strongly-coupled low-viscosity liquid-like system [6] and its lifetime at the energy densities reached at the LHC is of the order of 10 fm/c [7].

Heavy quarks, like charm and beauty, are mostly produced in primary hard scattering processes between the partons of the incoming nuclei, which occur in the early stages of the collisions. The time scales for heavy-quark production (≤ 0.07 fm/c for $c\bar{c}$ and ≤ 0.02 fm/c for $b\bar{b}$ pairs [8]) are shorter than the QGP formation time, which is about 0.3–1.5 fm/c at LHC energies [9]. Therefore, heavy quarks experience the full space–time evolution of the hot and dense QCD medium.

During their propagation in the QGP, heavy quarks interact with the medium constituents, by exchanging energy and momentum via elastic [10–12] and inelastic [13, 14] processes. Low-momentum heavy quarks (i.e. $\lesssim$ 3–4 GeV/c) mainly interact via elastic scatterings and are expected to acquire some collective behaviour of the system, like radial and anisotropic azimuthal flow, as a consequence of multiple interactions with the medium [15, 16]. The typical momentum exchange in the interactions of heavy quarks with the medium is small compared to the charm-quark mass. Therefore, heavy quarks undergo Brownian motion in the medium characterised by many small-momentum kicks. The degree of heavy-quark thermalisation provides unique insight into the thermalisation process of the system. Substantial theoretical efforts were made to describe the charm-quark transport in a hydrodynamically expanding medium [17]. The relevant transport parameter is the spatial diffusion coefficient D_s, which does not depend on the precise value of the heavy-quark mass and, hence, is a medium property. It can be estimated via the comparison of the measured differential yields as a function of transverse momentum (p_T) and azimuthal distributions of D mesons with model predictions.

For high-p_T quarks (i.e. $\gtrsim$ 8–10 GeV/c) the main manifestation of the interactions with the medium is energy loss, which can occur via collisional processes and gluon radiation [18], with the latter expected to be the dominant mechanism. In particular, the amount of radiative energy loss is influenced by the colour charge of the parton interacting with the medium. According to QCD calculations, gluons are expected to lose more energy than quarks, due to their stronger coupling to the medium [13, 14]. At LHC energies, light-flavour particles in the momentum interval $5 < p_T < 20$ GeV/c are expected to originate mostly from the fragmentation of gluons produced in hard scattering processes, while at higher p_T the contribution of light-quark jets becomes relevant [19]. On the other hand, charm mesons provide an experimental tag for a quark parent at all momenta. Thus, the comparison of heavy-flavour hadron production with that of light-flavour particles at high p_T can provide insight into this aspect. In addition, the energy loss of quarks can be affected by several mass-dependent effects like the dead-cone effect, which reduces the small-angle gluon radiation for quarks with moderate energy-over-mass values [20–23]. Similarly, collisional energy loss is predicted to depend on the quark mass and to be smaller for heavy quarks [24].

Heavy-flavour hadron yields and momentum distributions can be influenced by the modification of the parton distribution function (PDF) due to initial state effects, like nuclear shadowing [18]. It was also suggested that low-momentum heavy quarks could hadronise via recombination with other quarks from the medium, in addition to the fragmentation in the vacuum [16, 25].

The aforementioned effects can be investigated with the measurement of the nuclear modification factor R_{AA} of heavy-flavour hadrons. It is defined as the ratio of the p_T-differential production yield in nucleus–

2

nucleus collisions (dN_{AA}/dp_T) and the production cross section in proton–proton collisions (dσ_{pp}/dp_T) scaled by the average nuclear overlap function $\langle T_{AA} \rangle$

$$R_{AA}(p_T) = \frac{1}{\langle T_{AA} \rangle} \frac{\mathrm{d}N_{AA}/\mathrm{d}p_T}{\mathrm{d}\sigma_{pp}/\mathrm{d}p_T}, \qquad (1)$$

where $\langle T_{AA} \rangle$ is defined as the average number of binary nucleon–nucleon collisions ($\langle N_{coll} \rangle$), which can be estimated via Glauber model calculations [26–28], divided by the inelastic nucleon–nucleon cross section.

Measurements of prompt D-meson production were performed by the ALICE Collaboration in Pb–Pb collisions at $\sqrt{s_{NN}} = 2.76$ TeV [29] and 5.02 TeV [30] in the 0–10% and 30–50% centrality classes for both collision energies and in the 60–80% for the highest one. The D-meson yields show a suppression in central (0–10%) and semi-central (30–50%) collisions that reaches up to a factor of 5 and 2.5, respectively, at p_T of 6–10 GeV/c. It then decreases with increasing p_T, while the suppression factor is of 1.25 without a pronounced p_T dependence in peripheral (60–80%) collisions. The prompt D^0 production was also measured by the CMS Collaboration in the most central Pb–Pb collisions at $\sqrt{s_{NN}} = 5.02$ TeV [31] in the p_T range 2–100 GeV/c and the result is in agreement with ALICE measurements. Furthermore, also the STAR Collaboration measured the production of the prompt D^0 mesons in Au–Au collisions at $\sqrt{s_{NN}} = 200$ GeV [32] and the comparison with this result can provide insight into the $\sqrt{s}$ dependence of energy-loss effects. Conversely, the D-meson nuclear modification factor measured by the ALICE Collaboration in p–Pb collisions at $\sqrt{s_{NN}} = 5.02$ TeV [33], where an extended QGP is not expected to form, is compatible with unity for the whole measured p_T range.

Complementary information on the interactions of heavy quarks with the medium constituents and their possible thermalisation can be obtained from the measurements of the anisotropies in the D-meson azimuthal distributions, which are characterised in terms of the Fourier coefficients [34, 35]. In particular, the second order coefficient v_2, called elliptic flow, is defined as $v_2 = \langle \cos(2\varphi) \rangle$ where φ is the azimuthal angle. Recently, the ALICE Collaboration reported the latest measurements of prompt D-meson azimuthal anisotropic flow [36] in Pb–Pb collisions at $\sqrt{s_{NN}} = 5.02$ TeV.

In this paper, the measurements of the p_T-differential yields and nuclear modification factors of prompt D^0, D$^+$, and D^{*+} mesons (i.e. produced via the hadronisation of charm quarks or from the decays of excited charmed hadron states) and their charge conjugates, in central (0–10%) and semicentral (30–50%) Pb–Pb collisions at $\sqrt{s_{NN}} = 5.02$ TeV are reported. The statistical and systematic uncertainties have been reduced due to the Pb–Pb data sample collected with the ALICE detector at the end of 2018, that is larger by a factor eight (four) for central (semicentral) collisions with respect to the data sample collected in 2015 used for the previous publication [30], and to the production cross section measured in pp collisions at the same centre-of-mass energy [37]. The larger data sample allowed the reduction of the statistical uncertainties and the extension of the p_T reach of the measurements down to $p_T = 0$ for D^0 mesons. Moreover, the previous measurements [30] were affected by the uncertainty on the $\sqrt{s}$ scaling of the pp production cross section. The new measurements do not include such uncertainty since they use the measured pp production cross section at the same collision energy [37].

The paper is structured as follows. The data sample and the experimental apparatus are briefly introduced in Section 2. The D-meson reconstruction procedure and the corrections applied to the raw yields are presented in Section 3, while the estimation of the systematic uncertainties is described in Section 4. The results are presented in Section 5, together with a comparison with the charged-pion, proton, and prompt and non-prompt J/ψ R_{AA}, along with model calculations. In addition, a simultaneous comparison of the measured R_{AA} and elliptic flow v_2 [36] at low and intermediate p_T with transport-model calculations is discussed, together with an estimate of the spatial diffusion coefficient. This comparison will provide insights into the participation of the charm quark in the collective expansion of the medium [38], as well

Table 1: Average nuclear overlap function, number of events, and recorded integrated luminosities for the two centrality classes used in the analysis.

Centrality class	$\langle T_{AA} \rangle$ (mb^{-1})	N_{events}	$L_{int}(\mu b^{-1})$
0–10%	23.26 ± 0.17	100×10^6	130.5 ± 0.5
30–50%	3.92 ± 0.06	85×10^6	55.5 ± 0.2

as on the role of the different hadronisation mechanisms. Conclusions and perspectives are drawn in Section 6.

2 Detector and data sample

The ALICE experimental apparatus includes several detectors for particle tracking and identification as well as electromagnetic calorimeters at midrapidity ($|\eta| < 0.9$), a forward muon spectrometer ($-4 < \eta < -2.5$), and a set of forward and backward detectors used for triggering, background rejection, and event characterisation. A detailed description of the apparatus and its performance can be found in Refs. [39, 40].

The main detectors used for the track reconstruction and particle identification in the analysis are the Inner Tracking System (ITS) [41], the Time Projection Chamber (TPC) [42], and the Time-Of-Flight (TOF) detector [43]. They are located inside a large solenoidal magnet, providing a uniform magnetic field of 0.5 T parallel to the LHC beam direction. Charged-particle trajectories are reconstructed from their hits in the ITS and the TPC. The ITS consists of a six-layer silicon detector, which is used for tracking and for the reconstruction of primary and secondary vertices. The TPC is used for track reconstruction and particle identification (PID) via the measurement of the specific energy loss dE/dx. The TOF detector extends at intermediate momenta the PID capabilities of the TPC via the measurement of the time-of-flight of charged particles from the interaction point to the detector.

Event selection and characterisation are performed with the V0 detector [44] and the Zero Degree Calorimeter (ZDC) [45]. The V0 detector consists of two scintillator arrays, which cover the full azimuth in the pseudorapidity intervals $-3.7 < \eta < -1.7$ (V0C) and $2.8 < \eta < 5.1$ (V0A), and is used for triggering, event selection, and centrality determination. A minimum-bias interaction trigger was provided by the coincidence of signals in the V0A and the V0C. Furthermore, two separate trigger classes, which consist of an online event selection based on the V0 signal amplitude, were used during the 2018 Pb–Pb data taking period in order to enrich the sample of central and semicentral collisions. Events due to the interaction of the beams with residual gas in the vacuum pipe were rejected offline using the V0 and the ZDC timing information. Only events with a primary vertex reconstructed within ± 10 cm from the centre of the detector along the beam axis were considered in the analysis.

Collisions were divided into centrality classes, defined in terms of percentiles of the hadronic Pb–Pb cross section, using the sum of the V0 signal amplitudes, as described in details in Ref. [30]. The centrality classes used in the present analysis, together with the corresponding average nuclear overlap function $\langle T_{AA} \rangle$ [46, 47], the number of events (N_{events}), and the recorded integrated luminosity L_{int} [48] in each class, are summarised in Table 1.

3 Analysis techniques

3.1 D-meson raw yields

The D mesons and their charge conjugates were reconstructed via the following hadronic decay channels: $D^0 \rightarrow K^- \pi^+$ (with branching ratio, BR $= 3.950 \pm 0.031\%$), $D^+ \rightarrow K^- \pi^+ \pi^+$ (BR $= 9.38 \pm 0.16\%$), and $D^{*+} \rightarrow D^0 \pi^+$ (BR $= 67.7 \pm 0.5\%$) [49]. The analysis was based on the reconstruction of decay vertices

displaced from the primary vertex, exploiting the separation of few hundreds μm due to the weak decays of D^0 and D^+ ($c\tau$ of $\sim$ 123 and $\sim$ 312 μm, respectively [49]). In the case of the strong decay of the D^{*+} meson, the decay topology of the produced D^0 was exploited. This method allowed the reconstruction of D^0 candidates for $p_T > 1$ GeV/c in both centrality classes and of D^+ (D^{*+}) candidates for $p_T > 2.5$ (3) GeV/c and for $p_T > 2$ (2) GeV/c in the 0–10% and 30–50% centrality classes, respectively.

D^0 and D^+ candidates were built using pairs and triplets of tracks with proper charge-sign combination, $|\eta| < 0.8$, $p_T > 0.4$ GeV/c, a minimum number of two hits (out of six) in the ITS, with at least one in the two innermost layers, at least 70 out of 159 crossed TPC pad rows, and a fit quality $\chi^2/\text{ndf} < 1.25$ in the TPC (where ndf is the number of degrees of freedom involved in the track fit procedure). D^{*+} candidates were reconstructed by combining D^0 candidates with tracks, which were required to have $|\eta| < 0.8$, $p_T > 0.1$ GeV/c, and at least three associated hits in the ITS.

These track selection criteria reduce the D-meson acceptance in rapidity, which, depending on p_T, varies from $|y| > 0.5$ at low p_T and $|y| > 0.8$ for $p_T > 5$ GeV/c. Consequently, a p_T-dependent fiducial acceptance selection, $|y| < y_{\text{fid}}(p_T)$, was applied, with $y_{\text{fid}}(p_T)$ defined according to a second-order polynomial function increasing from 0.5 to 0.8 in the range $0 < p_T < 5$ GeV/c, and fixed to 0.8 for $p_T > 5$ GeV/c.

The D-meson selection strategy is similar to the one used in previous analyses and the variables used to distinguish between signal and background candidates are based on the impact parameters (i.e. the distance of closest approach between the track and the primary vertex in the plane transverse to the beam direction) of the decay particles, the separation of the primary and secondary vertices, and the pointing of the reconstructed D-meson momentum to the primary vertex, as described in Refs. [30, 50]. These selection criteria tend to enhance reconstructed feed-down D mesons, originating from beauty-hadron decays, over those promptly produced. An additional selection was therefore applied on the normalised difference between the measured and expected impact parameters of each of the decay particles, which allows for a significant rejection of background candidates and feed-down D mesons, while keeping a large fraction of prompt D mesons as reported in Ref. [51]. Further reduction of the combinatorial background was obtained by applying PID for charged pions and kaons with the TPC and TOF detectors. A $\pm 3\sigma$ window around the expected mean values of dE/dx and time-of-flight was used for the identification, where σ is the resolution on these two quantities. A tighter PID selection criterion ($\pm 2\sigma$) was used for D^+ (for $p_T < 3$ GeV/c) and D^{*+} candidate daughters in central collisions because of the large background of track triplets.

An alternative analysis method, not based on the reconstruction and selection of the displaced decay-vertex topology, was previously developed and applied for the two-body decay of D^0 mesons in pp and p–Pb collisions, in order to extend the measurement down to $p_T = 0$ [37, 52]. This technique, which is used for the first time in the analysis of Pb–Pb collisions, does not use geometrical selections on the displaced decay vertex (which are not effective at very low p_T), but relies mainly on particle identification and on the estimation and subtraction of the combinatorial background. The D^0 candidates were formed combining pairs of tracks with opposite charge sign (unlike sign, ULS), with $|\eta| < 0.8$ and $p_T > 0.4$ GeV/c. Single-track and particle identification selections as well as the fiducial acceptance selection of the reconstructed candidates were performed using the same strategy adopted in the analysis with decay-vertex reconstruction previously described. The contribution to the invariant-mass distribution of ULS Kπ pairs due to combinatorial background is estimated with the event-mixing technique. The events are grouped in pools, before the event-mixing, based on the primary vertex position along z and on the event multiplicity, quantified by the number of track segments reconstructed in the two innermost layers of the ITS. Then, the kaon tracks of a given event are mixed with the pion tracks of other events. The top left panel of Fig. 1 shows the invariant-mass distribution of ULS Kπ pairs together with that of the background estimated with the event-mixing technique in the interval $0 < p_T < 1$ GeV/c. The latter distribution was normalised to match the yield of ULS pairs at one edge of the invariant-mass interval
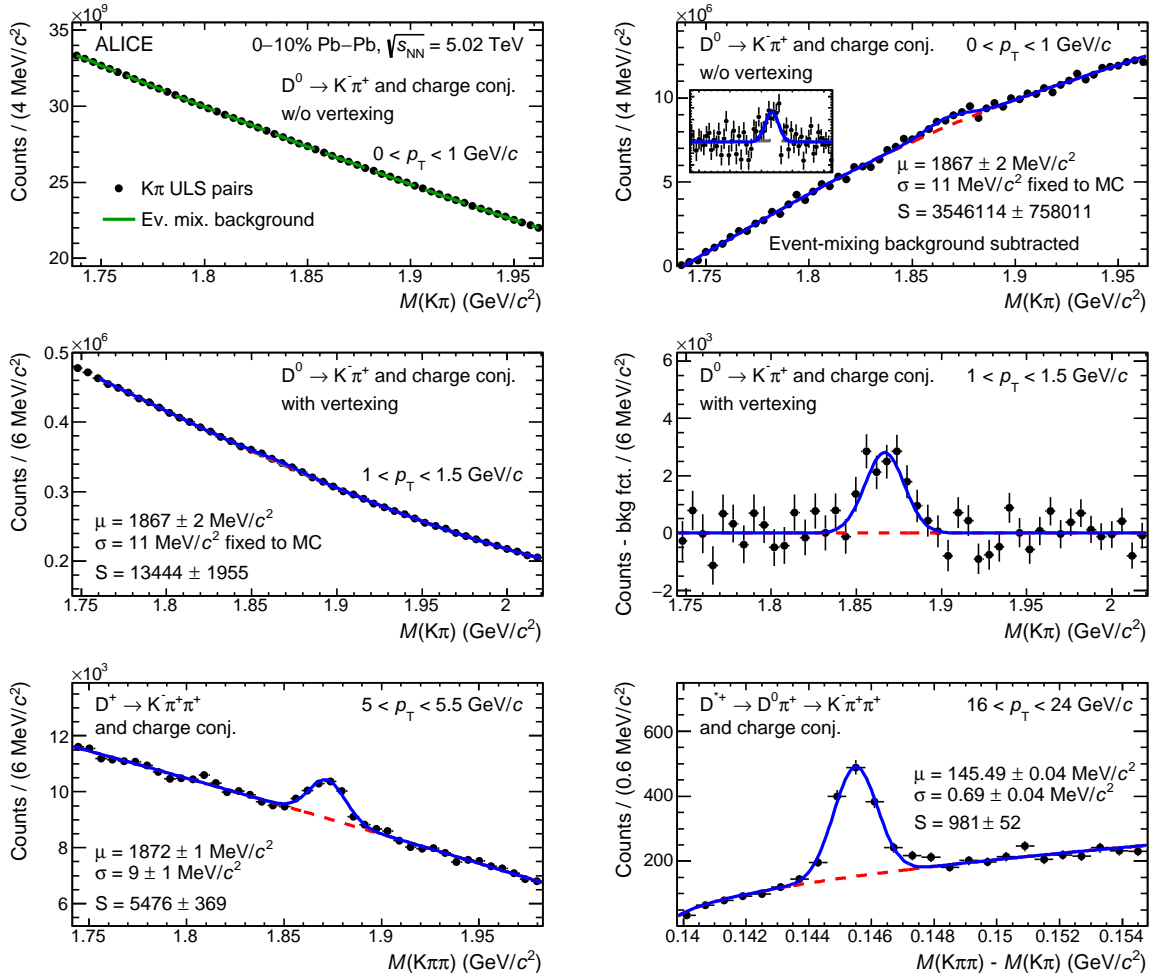
Figure 1: Invariant-mass (mass-difference) distribution of D^0, D^+, and D^{*+} meson candidates in different p_T intervals for the centrality class 0–10%. The fit functions are composed of a Gaussian function for the signal and an additional term for the background, as described in detail in the text. The values for the Gaussian mean μ, width σ, and raw yield S are also reported. Top row: D^0-meson candidates with $0 < p_T < 1$ GeV/c without reconstructing the decay vertex. The invariant-mass distributions are shown before (left) and after (right) the subtraction of the combinatorial background estimated from event-mixing. Middle row: D^0-meson candidates with $1 < p_T < 1.5$ GeV/c with reconstruction of the decay vertex before (left) and after (right) background subtraction. The width of the Gaussian in this and in the previous p_T interval is fixed to the value obtained from simulations. Bottom row: D^+-meson candidates with $5 < p_T < 5.5$ GeV/c (left) and D^{*+}-meson candidates with $16 < p_T < 24$ GeV/c (right).

considered for the extraction of the D^0 raw yield.

The D-meson raw yields, including particles and antiparticles, were obtained from binned maximum-likelihood fits to the D^0 and D^+ candidate invariant mass (M) distribution and to the mass difference $\Delta M = M(K\pi\pi) - M(K\pi)$ distribution for D^{*+} candidates. Figure 1 shows examples of fits for these distributions in the 0–10% centrality class and for four p_T intervals. In the analysis of the D^0 meson without decay-vertex reconstruction, the fit is performed after subtracting the estimated background from the ULS $K\pi$ invariant-mass distribution as shown in the top right panel.

The fit function was composed of a Gaussian term to describe the signal and an exponential function for the background for D^0 and D^+ candidates at intermediate and high p_T in the analysis with vertex

reconstruction. At low p_T ($p_T < 3$ GeV/c for D^0 and $p_T < 5$ GeV/c for D$^+$), a second-order polynomial function is used to model the background invariant-mass shape in both centrality classes. In the D^0 analysis without vertex reconstruction, instead, the background was parametrised for $p_T < (>)$ 2 GeV/c with a fourth-order (third-order) polynomial function. The ΔM distribution of D^{*+} candidates was fitted with a Gaussian function for the signal and the following function for the background: $a\sqrt{\Delta M - m_\pi}\mathrm{e}^{b(\Delta M - m_\pi)}$, where m_π is the pion mass and a and b are free parameters.

In some cases a D^0-meson candidate can be also identified as a $\overline{\mathrm{D}}^0$ meson when the two daughter tracks are compatible with both the kaon and pion hypothesis, leading to an irreducible correlated background. Hence, in the D^0 meson analyses, an additional term was included in the fit function to take into account this contribution to the invariant mass of signal candidates, which is called reflections. It was parametrised with a double-Gaussian distribution based on detailed Monte Carlo simulations. This contribution ranges between 2% and 3% of the raw signal depending on p_T [30]. Given the critical signal extraction for the D^0 meson at low p_T in the analysis with vertex reconstruction, due to the small signal-to-background ratio, the width of the Gaussian for the signal was fixed to the value obtained from the simulation for $p_T < 1.5$ GeV/c. We verified that the widths from the simulation were consistent with those extracted from the data. For the same reason, in the analysis without vertexing the Gaussian width was fixed to the one from the simulation in the whole p_T range. The statistical significance of the signal, defined as $S/\sqrt{S+B}$ where S is the raw signal yield obtained by integrating the Gaussian function and B is the background under the peak (within 3σ), varies from 4 to 60, depending on the D-meson species, the p_T interval, and the centrality class. In the D^0 analysis without decay-vertex reconstruction, the S/B in the p_T range 0–1 GeV/c is approximately $\sim 8.5 \times 10^{-6}$ before the mixed-event background subtraction.

3.2 Yield corrections and beauty feed-down subtraction

The D-meson raw yields were corrected to obtain the p_T-differential yields of prompt D-mesons according to:

$$\frac{\mathrm{d}^2 N}{\mathrm{d}y\,\mathrm{d}p_T} = \frac{1}{2}\frac{1}{\Delta p_T}\frac{f_{\mathrm{prompt}}(p_T) \times N_{\mathrm{raw}}^{\mathrm{D}+\overline{\mathrm{D}}}(p_T)\Big|_{|y|<y_{\mathrm{fid}}}}{\alpha_y(p_T) \times (\mathrm{Acc} \times \varepsilon)_{\mathrm{prompt}}(p_T) \times \mathrm{BR} \times N_{\mathrm{events}}}. \tag{2}$$

The raw yield values $N^{\mathrm{D}+\overline{\mathrm{D}},\mathrm{raw}}$, which contain the contribution of feed-down from beauty-hadron decays, were multiplied by the fraction of promptly produced D mesons f_{prompt} and divided by a factor of two to obtain the charged-averaged yields. Furthermore, they were divided by the product of prompt D-meson acceptance and efficiency $(\mathrm{Acc} \times \varepsilon)_{\mathrm{prompt}}$, the branching ratio BR of the decay channel, the width of the p_T interval (Δp_T), and by the number of events N_{evt}. The factor $\alpha_y(p_T)$ normalises the corrected yields measured in $\Delta y = 2y_{\mathrm{fid}}(p_T)$ to one unit of rapidity. It was computed as the ratio between the generated D-meson yield in $|y| < y_{\mathrm{fid}}(p_T)$ and that in $|y| < 0.5$ using a data-driven p_T shape and a rapidity distribution from fixed order plus next-to-leading logarithms (FONLL) [53,54] perturbative QCD calculations, after verifying that the D-meson rapidity distributions in FONLL are consistent with those from PYTHIA 8 [55].

The $(\mathrm{Acc} \times \varepsilon)$ correction was obtained separately for prompt and feed-down D mesons using simulations with the GEANT3 transport package [56], including a detailed description of the detector geometry and response as well as of the LHC beam conditions. The Pb–Pb collisions at $\sqrt{s_{\mathrm{NN}}} = 5.02$ TeV were produced with the HIJING v1.36 [57] event generator and D-meson signals were added by injecting $c\overline{c}$ or $b\overline{b}$ pairs generated with the PYTHIA v8.2.43 event generator with Monash tune [58]. The D-meson p_T distributions from the simulations were reweighted in order to use realistic momentum distributions in the determination of the acceptance and the efficiency, which depend on p_T. The weights were defined with an iterative procedure to match the p_T dependence measured for D^0 mesons in the intervals used in the analysis, for both centrality classes and in the momentum interval $1 < p_T < 50$ GeV/c.

Figure 2 shows the $(\mathrm{Acc} \times \varepsilon)$ for prompt and feed-down D^0 (top panels), D$^+$ (bottom left panel), and
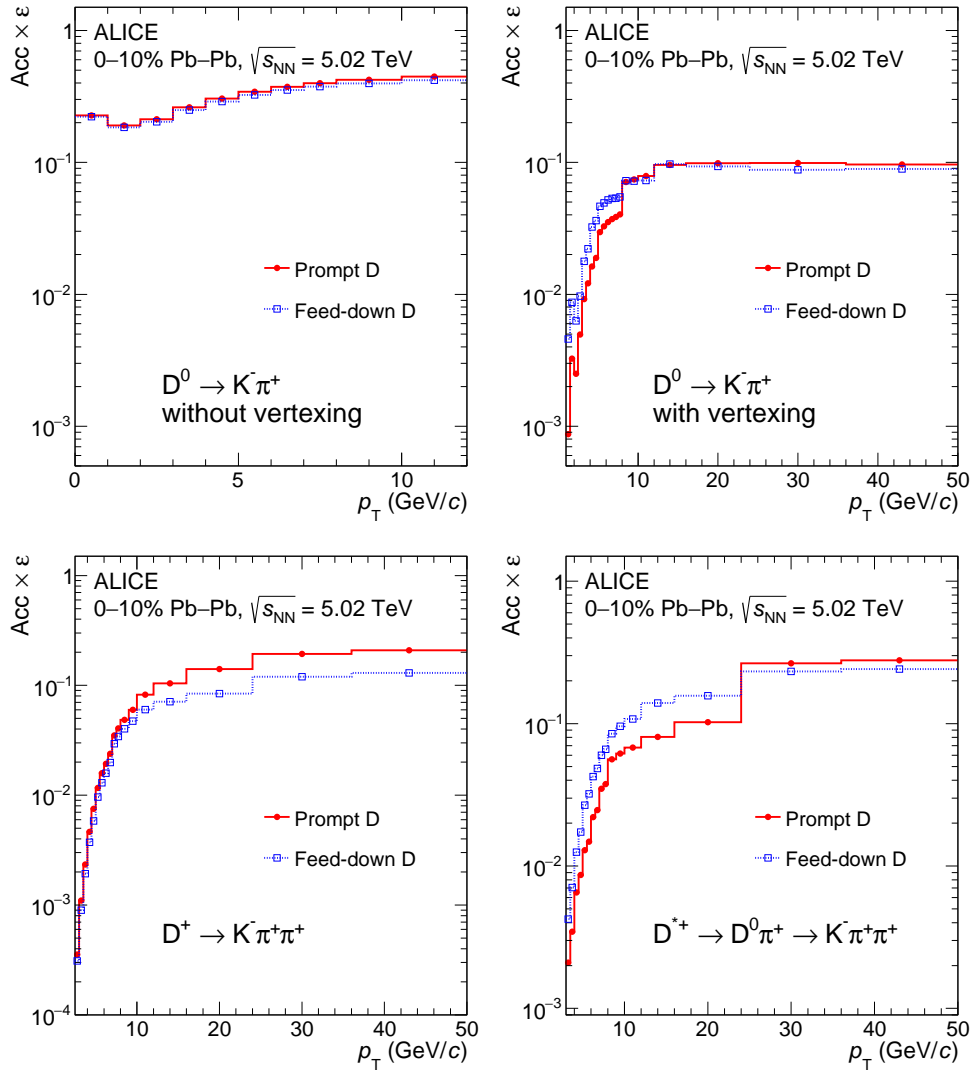
Figure 2: Product of acceptance and efficiency (Acc × ε) as a function of p_{T} for prompt (red circles) and feed-down (blue squares) D mesons in Pb–Pb collisions for the 0–10% centrality class.

D*⁺ (bottom right panel) mesons with $|y| < y_{\mathrm{fid}}$ as a function of p_{T} in the 0–10% centrality class. For the analysis that does not exploit the selections on the D⁰-meson decay vertex (top left panel), the efficiency is higher by a factor of about 100 (5) at low (high) p_{T} as compared to the analysis with decay-vertex reconstruction (top right panel). The (Acc × ε) is almost independent of p_{T} (the mild increase with increasing p_{T} is mainly determined by the geometrical acceptance of the detector) and is the same for prompt and feed-down D⁰, as expected when no selection is made on the displacement of the D⁰-meson decay vertex from the interaction point.

The efficiencies for the analysis with geometrical selections on the displaced decay-vertex topology range from about 10^{-3} at low p_{T} to 0.1–0.3 at high p_{T}, depending on the D-meson species. The decreasing efficiency with decreasing p_{T} is due to the fact that more stringent selection criteria are needed at low p_{T} because of the larger background and the smaller average displacement of the decay vertex from the interaction point. The trend of the efficiency with p_{T} is not completely smooth, especially for D⁰ and D*⁺, reflecting the p_{T} intervals in which the optimisation of the selection criteria was performed. The (Acc × ε) is higher for semicentral collisions than for central collisions, since less stringent selections are applied because of the lower combinatorial background. The difference between the efficiencies

for prompt and feed-down D mesons is due to the geometrical selections applied since the latter are more displaced from the primary vertex due to large B-meson lifetime ($\tau \approx 500\ \mu$m) and are therefore more efficiently selected by the majority of the selection criteria applied in the analysis. However, the requirement on the difference between measured and expected decay track impact parameter rejects efficiently D mesons coming from beauty-hadron decays. This is particularly effective for D$^+$ mesons (Fig. 2 bottom left panel) whose feed-down efficiencies become lower than the prompt efficiencies after a selection on the aforementioned variable is applied.

The fraction of prompt D mesons f_{prompt} was obtained with the procedure introduced in Refs. [30, 59] to account for the contribution of D mesons from beauty-hadron decays in the measured raw yield. The f_{prompt} factor was estimated in each p_{T} interval using perturbative QCD calculations for the cross section of feed-down D mesons, efficiencies from the simulations, and a hypothesis on the R_{AA} of feed-down D mesons. In detail, the expression for f_{prompt} is:

$$
f_{\text{prompt}} = 1 - \frac{N_{\text{raw}}^{\text{D}+\overline{\text{D}}\,\text{feed-down}}}{N_{\text{raw}}^{\text{D}+\overline{\text{D}}}}
$$

$$
= 1 - R_{AA}^{\text{feed-down}} \times \langle T_{AA} \rangle \times \left(\frac{d\sigma}{dp_{\text{T}}} \right)_{\text{feed-down},\,|y|<0.5}^{\text{FONLL, PYTHIA 8}} \times \frac{2\Delta p_{\text{T}} \times \alpha_y \times (\text{Acc} \times \varepsilon)_{\text{feed-down}} \times \text{BR} \times N_{\text{events}}}{N_{\text{raw}}^{\text{D}+\overline{\text{D}}}},
$$

(3)

where $N_{\text{raw}}^{\text{D}+\overline{\text{D}}}$ is the measured raw yield and $N_{\text{raw}}^{\text{D}+\overline{\text{D}}\,\text{feed-down}}$ is the estimated raw yield of D mesons from beauty-hadron decays. The beauty-hadron production cross section in pp collisions at $\sqrt{s} =$ 5.02 TeV, estimated with FONLL calculations [60], was folded with the beauty-hadron$\rightarrow$ D$+X$ decay kinematics from PYTHIA 8 and multiplied by the $(\text{Acc} \times \varepsilon)$ of feed-down D mesons, by the $\langle T_{AA} \rangle$ of the corresponding centrality class, and by the other factors introduced in Eq. 2. Finally, the nuclear modification factor of D mesons from beauty-hadron decays ($R_{AA}^{\text{feed-down}}$) was accounted for.

The comparison of the R_{AA} of prompt D mesons (R_{AA}^{prompt}) at $\sqrt{s_{\text{NN}}} = 5.02$ TeV [30] with that of J/ψ from B-meson decays at the same energy measured by the CMS [61] and the ATLAS [62] collaborations indicates that prompt charmed hadrons are more suppressed than non-prompt charmed hadrons. The difference between the R_{AA} values is about a factor two in central collisions at a p_{T} value of about 10 GeV/c [30] and it is described by model calculations with parton-mass-dependent energy loss. Therefore, for the centrality classes 0–10% and 30–50%, the value $R_{AA}^{\text{feed-down}} = 2 \times R_{AA}^{\text{prompt}}$ was assumed to compute the f_{prompt} factor for D mesons with $3 < p_{\text{T}} < 24$ GeV/c. To estimate a systematic uncertainty, this hypothesis was varied in the range $1 < R_{AA}^{\text{feed-down}}/R_{AA}^{\text{prompt}} < 3$ considering the data uncertainties and model variations. For $p_{\text{T}} < 3$ GeV/c and $24 < p_{\text{T}} < 50$ GeV/c, since model calculations predict a lower difference between R_{AA}^{prompt} and $R_{AA}^{\text{feed-down}}$ [63, 64], the hypothesis $R_{AA}^{\text{feed-down}} = 1.5 \times R_{AA}^{\text{prompt}}$ was used, with a variation in the range $1 < R_{AA}^{\text{feed-down}}/R_{AA}^{\text{prompt}} < 2$ for estimating the systematic uncertainty.

The resulting values of the f_{prompt} factor, for the central hypotheses on $R_{AA}^{\text{feed-down}}/R_{AA}^{\text{prompt}}$, range from about 0.80 to 0.95, depending on the D-meson species, centrality class, and p_{T} interval. The values of f_{prompt} for the D^0 analysis without decay-vertex reconstruction are larger compared to those from the analysis with geometrical selections since the feed-down component is not enhanced by the topological selection criteria. The systematic uncertainties obtained from the variation of the hypotheses are discussed in Section 4.

4 Systematic uncertainties

The systematic uncertainties on the corrected yields of D^0, D$^+$, and D^{*+} mesons were estimated as a function of p_{T} for the 0–10% and 30–50% centrality classes considering the following sources: (i) extraction of the raw yield from the invariant-mass distributions; (ii) reconstruction efficiency of the

Table 2: Relative systematic uncertainties on prompt D-meson yields in Pb–Pb collisions at $\sqrt{s_{NN}} = 5.02$ TeV for representative p_T intervals. The first p_T interval of the D^0 corresponds to the analysis without decay vertex reconstruction. For the uncertainties on the correction factors, values below 0.5% are considered negligible.

Particle		D^0			D$^+$		D^{*+}	
p_T interval (GeV/c)		0–1	1.5–2	7.5–8	3–3.5	7.5–8	3–3.5	7.5–8
0–10% centrality	Raw-yield extraction	9%	7%	2%	5%	5%	7%	3%
	Correction factor							
	Tracking efficiency	8%	9%	9%	14%	15.5%	13%	9%
	Selection efficiency	negl.	8%	2%	5%	5%	13%	4%
	PID efficiency	negl.	negl.	negl.	negl.	negl.	1%	1%
	MC p_T shape	negl.	0.5%	negl.	negl.	negl.	0.5%	negl.
	Feed-down from beauty	$^{+2.7}_{-2.9}$%	$^{+7.6}_{-8.3}$%	$^{+11.6}_{-12}$%	$^{+3.4}_{-3.2}$%	$^{+7.1}_{-6.6}$%	$^{+8.4}_{-8.1}$%	$^{+10.3}_{-10.3}$%
	Branching ratio	0.8%			1.7%		1.1%	
	Centrality limits	<0.1%						
30–50% centrality	Raw-yield extraction	11%	4%	2%	4%	3%	5%	4%
	Correction factor							
	Tracking efficiency	7%	7.5%	7%	11%	11%	10%	9%
	Selection efficiency	negl.	8%	2%	4%	3%	9%	4%
	PID efficiency	negl.	negl.	negl.	negl.	negl.	negl.	negl.
	MC p_T shape	negl.	1%	negl.	negl.	negl.	negl.	negl.
	Feed-down from beauty	$^{+2.7}_{-2.9}$%	$^{+9.6}_{-10.4}$%	$^{+11.4}_{-11.7}$%	$^{+3.4}_{-3.2}$%	$^{+6.6}_{-6.3}$%	$^{+8.5}_{-8.2}$%	$^{+9.9}_{-9.9}$%
	Branching ratio	0.8%			1.7%		1.1%	
	Centrality limits	2%						

decay-particle tracks; (iii) D-meson selection efficiency; (iv) PID efficiency; (v) generated D-meson p_T and rapidity shape; (vi) subtraction of the contribution originating from beauty-hadron decays. In addition, a global normalisation uncertainty due to the branching-ratio uncertainty and the centrality interval determination was considered. The estimated values of the systematic uncertainties are summarised in Table 2 for the three D-meson species in representative p_T intervals.

The systematic uncertainty on the D-meson raw yield was estimated in each p_T interval by varying the invariant-mass interval considered in the fit and the functional form of the background fit function. The sensitivity to the line shape of the signal was tested by considering the raw yield values obtained by counting the candidates in the invariant-mass region of the signal peak after subtracting the background estimated from the side bands. In the case of the D^0-meson analysis without decay-vertex reconstruction, an additional contribution related to the line shape of the signal was estimated by varying the width of the Gaussian function by ±10% with respect to the Monte Carlo expectation, based on the deviations between the Gaussian width values observed in data and simulations for the analysis with decay-vertex reconstruction. The systematic uncertainty was defined as the RMS of the distribution of the signal yields obtained from all these variations. In the case of D^0 mesons, an additional contribution due to the modelling of the reflection contribution in the fit was estimated by varying (by ±20%) the ratio of the integral of the reflections to the integral of the signal and the shape of the templates used in the invariant-mass fits. The assigned uncertainty ranges from 2% to 11% depending on the D-meson species and p_T interval, being on average smaller in the 30–50% centrality class due to the larger signal-to-background

ratio in this class as compared to central collisions.

The systematic uncertainty on the track reconstruction efficiency has two contributions. The first one was estimated by varying the track quality selection criteria. The second contribution originates from possible differences in the probability to match the TPC tracks to the ITS hits in data and in simulations. It was estimated by comparing the matching efficiency in data and simulations after weighting the relative abundances of primary and secondary particles in the simulation to match those observed in data. The uncertainty was estimated for the single track and propagated to the reconstructed D mesons using the decay kinematics. The estimated uncertainty is the quadratic sum of the two contributions and it depends on the D-meson species and p_T, ranging from 3% to 10.5% for the two-body decay of D^0 mesons and from 5.5% to 15.5% for the three-body decays of D^+ and D^{*+} mesons.

The uncertainty on the D-meson selection efficiency originates from imperfections in the description of the D-meson kinematic properties and of the detector resolution and alignment in the simulation. For the analyses with decay-vertex reconstruction, the systematic uncertainty was estimated by comparing the corrected yields obtained by repeating the analysis with different sets of selection criteria resulting in a significant modification of the raw yields, signal-to-background ratios, and efficiencies. The estimated uncertainty depends on the D-meson species and p_T interval, being larger at low p_T and for central collisions, where more stringent selections are used to obtain a good statistical significance of the signal. The values obtained in these analyses range from 2% (3%) to 8% (13%) for the two-(three-) body decay channel. In the case of the D^0-meson analysis without decay-vertex reconstruction, no geometrical selections on the displaced decay-vertex topology are applied, and the efficiencies are higher than those of the analysis with decay-vertex reconstruction and almost independent of p_T. The stability of the corrected yield was tested against variations of the single-track p_T selection and no systematic effect was observed.

The uncertainty on the PID selection efficiency was estimated by repeating the analyses with decay-vertex reconstruction without applying the PID selections. The resulting corrected yields were found to be compatible with those obtained with the PID selection and therefore no systematic uncertainty was assigned. For the D^0-meson analysis without decay-vertex reconstruction, the analysis without applying PID selections could not be performed due to the insufficient statistical significance of the signal. More stringent PID criteria (at 2σ level on TPC, or TOF or both) were tested and compatible values for the corrected yields were obtained. Based on this result and on the fact that the PID selections are the same as used in the analysis with decay-vertex reconstruction, no uncertainty due to PID was assigned. In the case of the D^{*+} analysis, more stringent PID selection criteria were used in the 0–10% centrality class. A systematic uncertainty of 1% was estimated by comparing the pion and kaon PID selection efficiencies in the data and in the simulation and combining the observed differences using the D^{*+}-meson decay kinematics. For this study, pure pion samples were selected from strange-hadron decays, while pure kaon samples in the TPC (TOF) were obtained using a tight PID selection in the TOF (TPC).

An additional contribution to the systematic uncertainty on the efficiency originates from a possible difference between the real and simulated D-meson p_T and rapidity distributions. The effect of the p_T shape was estimated by calculating the efficiency using alternative D-meson transverse momentum shapes via a reweighting technique. In particular, the p_T distributions from FONLL calculations with and without hot-medium effects parametrised based on the R_{AA} in central collisions from different models were considered. For the analyses with decay-vertex reconstruction, the resulting uncertainty, which also includes the effect of the p_T dependence of the nuclear modification factor, was estimated to be negligible for $p_T > 5$ GeV/c and to increase to 1–1.5% in the lowest p_T intervals considered in the analysis, where the efficiency varies steeply with p_T. Instead, no sensitivity to the generated D^0 p_T shape was observed in the results of the D^0-meson analysis without decay-vertex reconstruction. The simulated rapidity shape of D mesons affects the Acc $\times \varepsilon$ and the α_y factors in the calculation of the cross section. It was verified that the D-meson rapidity distributions in the PYTHIA 8 simulations and FONLL calculations

are similar, resulting in a negligible effect on the Acc × ε and α_y correction factors. For the latter factor, an extreme assumption of a flat rapidity shape was tested and the difference with respect to the FONLL case was found to be smaller than 1% for $p_T < 10$ GeV/c and to be smaller than 2% at higher p_T. Considering that at high p_T the assumption of a flat rapidity shape is an extreme variation, the effect of the generated dN/dy shape was considered to be negligible and no systematic uncertainty was assigned.

The systematic uncertainty on the f_{prompt} correction factor was estimated by varying (i) the FONLL parameters (b-quark mass and factorisation and renormalisation scales, according to the prescription in Ref. [60]) in the calculation of the p_T-differential production cross section of feed-down D mesons, and (ii) the ratio between the feed-down and prompt D-meson R_{AA}, as described above. The resulting uncertainty ranges between 2% and 14%, depending on the D-meson species and p_T and centrality interval.

The normalisation uncertainty due to the centrality interval definition was estimated from the variation of raw yield observed when varying the limits of the centrality classes to account for the uncertainty on the fraction of the hadronic cross section used in the Glauber fit to determine the centrality percentiles (see Ref. [65] for details).

In the calculation of the nuclear modification factor, the systematic uncertainties on the D-meson yield in Pb–Pb collisions and on the pp reference cross section were propagated as uncorrelated, except for the uncertainty on the BR, which cancels out in the ratio, and the contribution to the feed-down uncertainty originating from the variation of the parameters of the FONLL calculation, which was considered to be fully correlated between the Pb–Pb and pp measurements. In particular, the contributions of the uncertainties on (i) the normalisation of the pp cross section (due to the luminosity determination), (ii) the centrality limits of the Pb–Pb samples, and (iii) the $\langle T_{AA} \rangle$ estimated with the Glauber model are common to all the p_T intervals and therefore they constitute a normalisation uncertainty on the R_{AA}, which is shown separately from the other sources when displaying the results.

5 Results

5.1 Transverse-momentum-differential yields

In this section, the results on the p_T-differential (d^2N/dydp_T) and p_T-integrated (dN/dy) yields of prompt D^0, D^+, and D^{*+} mesons at midrapidity in Pb–Pb collisions at $\sqrt{s_{\text{NN}}} = 5.02$ TeV in the 0–10% and 30–50% centrality classes are presented. In the case of the D^0 mesons, two results for the d^2N/dydp_T were obtained from the analyses with and without selections on the decay-vertex topology. They are compared in Fig. 3, with the inset showing their ratio in the common p_T range. In the calculation of the ratio, the results in the narrower p_T intervals of the analysis with decay-vertex reconstruction were merged together to match the binning of the analysis without vertexing, and the systematic uncertainties were propagated treating the raw yield extraction as uncorrelated between the two analyses, and all the other sources of uncertainty as correlated. The vertical error bars represent the statistical uncertainties and the systematic uncertainties are depicted as boxes except for the BR uncertainty, which is reported separately. The symbols, representing the data points, are positioned horizontally at the center of each interval and the horizontal bars represent the width of the p_T interval. This convention is adopted in all the figures shown in this section.

The two results for the p_T-differential yield of prompt D^0 mesons are found to be consistent within statistical uncertainties, which are independent between the two analysis techniques because of the largely different signal-to-background ratios and efficiencies. The usage of these two techniques allows the measurement of the D^0 p_T-differential yields in a wide transverse momentum range extending down to $p_T = 0$ for the first time in Pb–Pb collisions. The most precise measurement of the prompt D^0-meson p_T spectrum, which will be shown and used for comparisons throughout the paper, is obtained by using
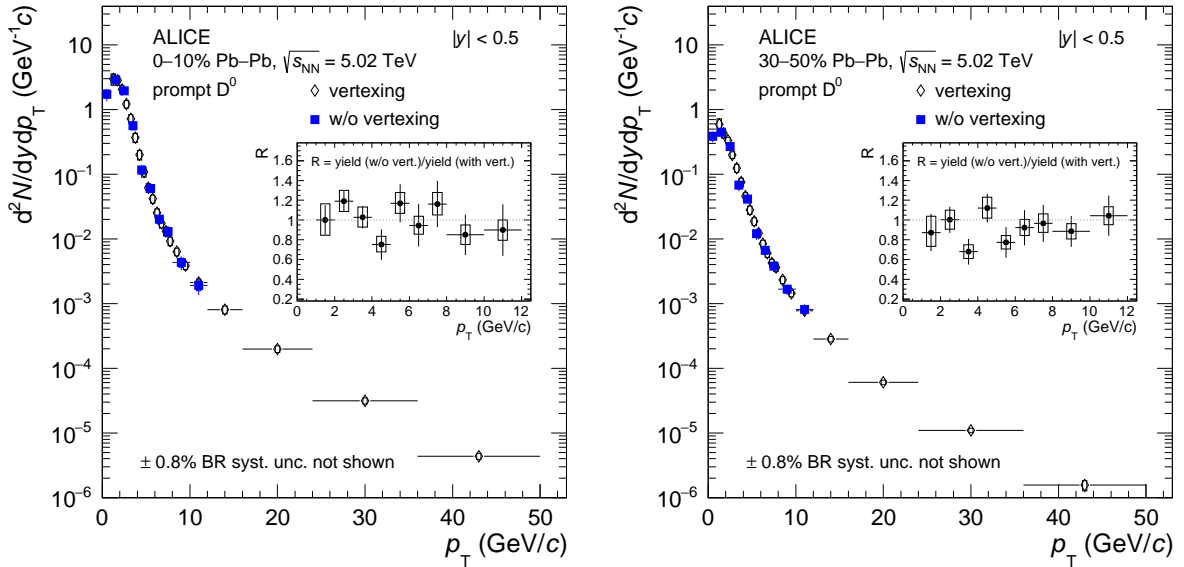
Figure 3: Transverse momentum distributions d^2N/dydp_T of prompt D^0 mesons from the analysis with (open marker) and without (full marker) decay-vertex reconstruction in the 0–10% and 30–50% centrality classes in Pb–Pb collisions at $\sqrt{s_{NN}}$ = 5.02 TeV. Statistical uncertainties (bars) and systematic uncertainties (boxes) are shown.

the results of the analysis without decay-vertex reconstruction in the p_T interval $0 < p_T < 1$ GeV/c and those from the analysis with decay-vertex reconstruction for $p_T > 1$ GeV/c.

The p_T-differential yields d^2N/dydp_T of prompt D^0, D$^+$, and D^{*+} mesons are shown in Fig. 4 for the 0–10% and 30–50% centrality classes. They are compared with the reference yields from pp collisions, which are computed as $\langle T_{AA} \rangle \times$ dσ_{pp}/dp_T, where dσ_{pp}/dp_T is the D-meson p_T-differential cross section measured in pp collisions at $\sqrt{s}$ = 5.02 TeV [37, 66], and $\langle T_{AA} \rangle$ is the average nuclear overlap function [47]. The D-meson production cross sections in pp collisions are measured up to 36 GeV/c and they are extrapolated with FONLL towards higher p_T, with the method described in Refs. [30, 65]. The spectra in the 30–50% centrality class are scaled by the factor reported in the legend for visibility. A clear suppression of the production yield for $p_T > 3$ GeV/c is visible in Pb–Pb collisions and it is stronger in central than in semicentral collisions.

Figure 5 shows the p_T-dependent ratios of the production yields of prompt D$^+$ and D^{*+} mesons relative to the D^0 ones, in the left panels, compared with the values measured in pp collisions at $\sqrt{s}$ = 5.02 TeV [37]. The systematic uncertainties were propagated to the ratios, considering the contributions from the tracking efficiency and the beauty-hadron feed-down subtraction as fully correlated among the different D-meson species. The values obtained in Pb–Pb and pp collisions are compatible within uncertainties and this indicates there is no modification of the relative abundances of D^0, D$^+$, and D^{*+} mesons as a function of p_T and for different centrality classes. The D$^+$/D^0 and D^{*+}/D^0 ratios are described within uncertainties by the GSI–Heidelberg statistical hadronisation model (SHMc) [67, 68] (right panels of Fig. 5), which predicts the p_T spectra of charm hadrons with a core–corona approach. The low-p_T region is dominated by the core contribution described with a blast-wave function, while the corona contribution is more relevant at high p_T and is parametrised from pp measurements. The rise predicted by the model, especially for D^{*+}/D^0, are due to the different D-meson masses and to the collective radial expansion of the system.

The visible production yields of prompt D^0, D$^+$, and D^{*+} mesons in the two centrality classes were evaluated by integrating the d^2N/dydp_T over the p_T intervals of the measurements. The results are
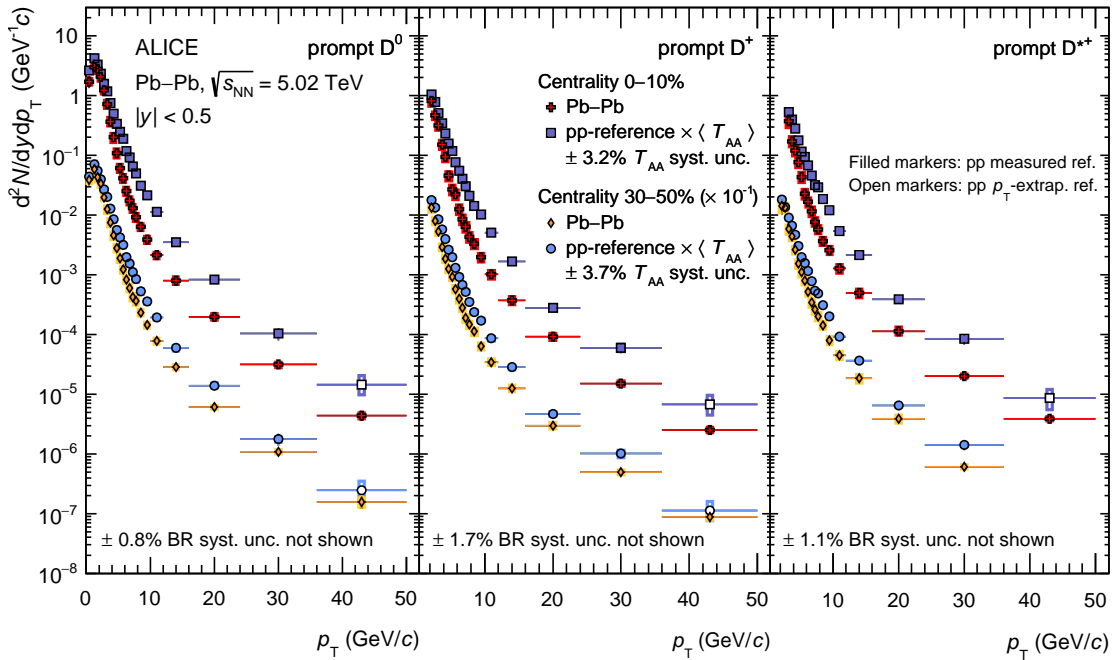
Figure 4: Transverse momentum distributions $d^2N/dydp_T$ of prompt D^0 (left), D^+ (middle), and D^{*+} (right) mesons in the 0–10% (circle) and 30–50% (square) centrality classes in Pb–Pb collisions at $\sqrt{s_{NN}} = 5.02$ TeV. The reference pp distributions multiplied by $\langle T_{AA} \rangle$ are shown as well. Statistical uncertainties (bars) and systematic uncertainties (boxes) are shown. The uncertainties on the BRs are quoted separately and the horizontal bars represent bin widths. The spectra in the 30–50% centrality class are scaled by the factor reported in the legend for visibility. Filled and empty markers of the pp reference indicate the measured [37, 66] and p_T-extrapolated values, respectively, of the p_T-spectrum.

reported in Table 3. For the yield integration, the systematic uncertainty was propagated assuming all sources of uncertainty as fully correlated among p_T intervals, except for the one on the raw-yield extraction, which was treated as uncorrelated because of the bin-to-bin variations of S/B and background invariant-mass shape.

The production yield of prompt D mesons per unit of rapidity, dN/dy, was obtained by extrapolating (where needed) the visible cross section to the full p_T range. Since the p_T-differential yields of D^0 mesons in the 0–10% and 30–50% centrality classes were measured down to $p_T = 0$, it was possible to obtain the dN/dy at midrapidity for the first time in Pb–Pb collisions at the LHC without using models or assumptions to extrapolate the p_T-differential yield to unmeasured momentum range at low p_T. Conversely, the dN/dy of D^+ and D^{*+} mesons were obtained via an extrapolation procedure exploiting the measured p_T-differential ratios relative to the D^0 meson. The measured p_T-differential D^+/D^0 and D^{*+}/D^0 ratios, shown in Fig. 5, were fit with two different functions (a constant and a constant plus logarithmic function) in order to extrapolate the ratios in the interval $0 < p_T < 2$ GeV/c, where the yields could not be measured. The extrapolation in the high-p_T range is negligible because the fraction of D-meson yield in central (semicentral) collisions with $p_T > 50$ (36) GeV/c is negligible. The yields of D^+ and D^{*+} mesons in the interval $0 < p_T < 2$ GeV/c were obtained by multiplying the measured D^0 yield in this p_T interval by the extrapolated ratio from the fit function. For the D^+/D^0 ratios, which show a flat trend as a function of p_T, the fit to a constant was used in the determination of the central value of the D^+ yield, while for the D^{*+}/D^0 ratio the fit with a constant plus a logarithmic function was used. The systematic uncertainty due to the extrapolation was estimated by evaluating the yields using the other fit function and the shape of the SHMc predictions with normalisation parameter left free. The
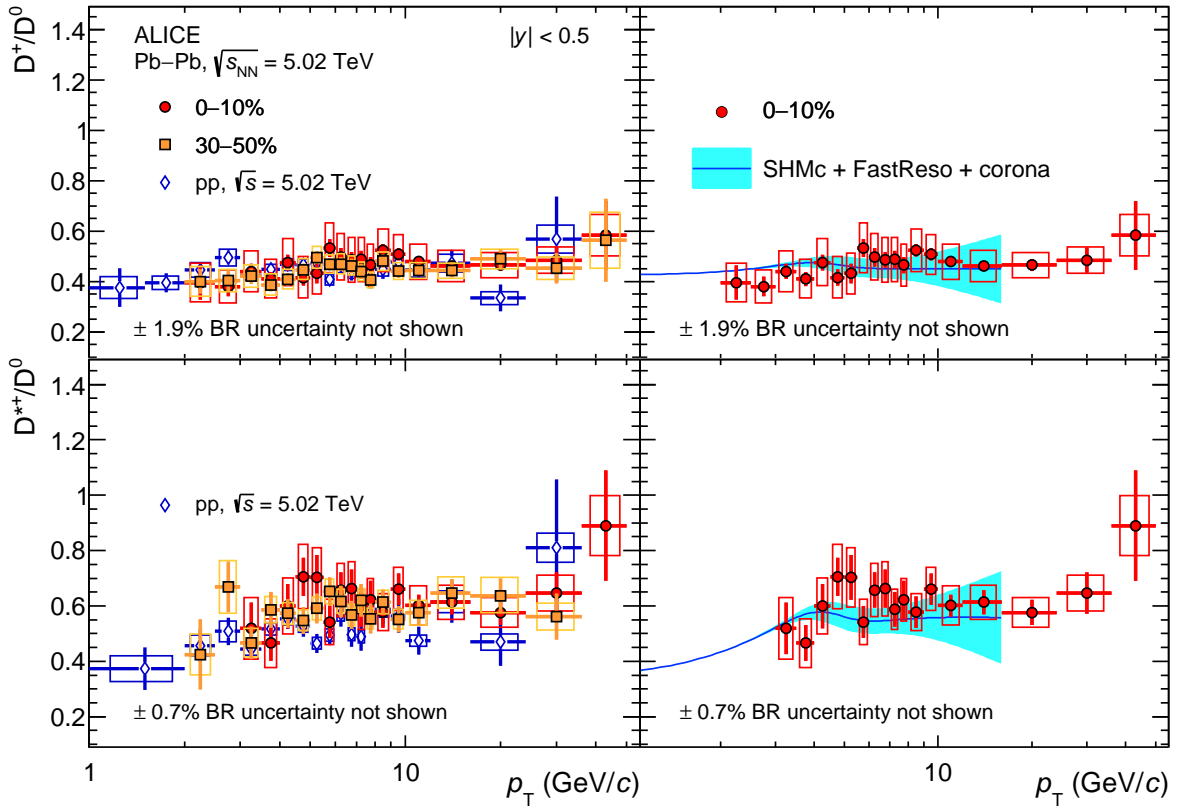
Figure 5: D^+/D^0 (top left panel) and D^{*+}/D^0 (bottom left panel) ratios as a function of p_T in central and semicentral Pb–Pb collisions compared to the results obtained from pp collisions [37]. The right panels show the ratios in central Pb–Pb collisions compared to the predictions from the statistical hadronisation model (SHMc) [67, 68] with a core–corona approach and the FastReso package [69] for resonance decays. Statistical (bars) and systematic (boxes) uncertainties are shown.

difference between the central value and the yields obtained with other functions for the extrapolation was assigned as systematic uncertainty and summed in quadrature to the uncertainty on the D^0 yield in the aforementioned p_T interval. The results for the prompt D-meson production yields per unit of rapidity dN/dy in $|y| < 0.5$ are reported in Table 4. In the case of the D^0 meson, the result coincides with the visible yield because the measurement extends down to $p_T = 0$ and the contribution of D^0 mesons with $p_T > 50$ (36) GeV/c is negligible.

In the right column the dN/dy values predicted by the SHMc [67, 68] are reported. In the SHMc approach, the yield of hadrons containing charm quarks can be calculated utilising as input values (i) the temperature T_{chem}, (ii) the volume of the fireball at the chemical freeze-out estimated from a fit to light-flavour hadron yields, and (iii) the number of $c\bar{c}$ pairs produced in the Pb–Pb collision. The latter was calculated from the charm-quark production cross section estimated from measurements in pp and p–Pb collisions along with guidance from parameterisations of the nuclear modification of the PDFs [70]. The SHMc calculations agree with the measurements within uncertainties, even though the data lie on the upper edge of the uncertainty band of the theoretical predictions, which is related to the uncertainty on the total charm production cross section used in the calculation. It is useful to note that the charm production cross section in pp collisions, which was used to determine the charm content of the fireball in the SHMc calculations, is lower than the recent measurement reported in Ref. [71] and therefore the yields from the SHMc would increase if the measured cross section were used as the input to the calculations. However, a firmer conclusion on the SHMc predictions for charm hadrons will be

Table 3: Visible production yield of prompt D^0, D$^+$, and D^{*+} mesons in $|y| < 0.5$ in the 0–10% and 30–50% centrality classes of Pb–Pb collisions at $\sqrt{s_{NN}} = 5.02$ TeV.

	Kinematic range	Visible production yield
		0–10% centrality
D^0	$0 < p_T < 50$ GeV/c	6.819 ± 0.457 (stat.) $^{+0.912}_{-0.936}$ (syst.) ± 0.054 (BR)
D$^+$	$2 < p_T < 50$ GeV/c	0.992 ± 0.073 (stat.) $^{+0.154}_{-0.155}$ (syst.) ± 0.017 (BR)
D^{*+}	$3 < p_T < 50$ GeV/c	0.438 ± 0.037 (stat.) $^{+0.084}_{-0.085}$ (syst.) ± 0.005 (BR)
		30–50% centrality
D^0	$0 < p_T < 50$ GeV/c	1.275 ± 0.099 (stat.) $^{+0.167}_{-0.173}$ (syst.) ± 0.010 (BR)
D$^+$	$2 < p_T < 50$ GeV/c	0.179 ± 0.008 (stat.) $^{+0.024}_{-0.024}$ (syst.) ± 0.003 (BR)
D^{*+}	$2 < p_T < 36$ GeV/c	0.230 ± 0.023 (stat.) $^{+0.038}_{-0.039}$ (syst.) ± 0.002 (BR)

Table 4: Measured p_T-integrated yields of prompt D^0, D$^+$, and D^{*+} in $|y| < 0.5$ in the 0–10% and 30–50% centrality classes of Pb–Pb collisions at $\sqrt{s_{NN}} = 5.02$ TeV. The right column reports the dN/dy predicted by the GSI–Heidelberg statistical hadronisation model [67, 68].

	Measured dN/dy	SHMc dN/dy
	0–10% centrality	
D^0	6.819 ± 0.457 (stat.) $^{+0.912}_{-0.936}$ (syst.) ± 0.054 (BR)	6.42 ± 1.07
D$^+$	3.041 ± 0.073 (stat.) $^{+0.154}_{-0.155}$ (syst.) ± 0.052 (BR) $^{+0.352}_{-0.618}$ (extrap.)	2.84 ± 0.47
D^{*+}	3.803 ± 0.037 (stat.) $^{+0.084}_{-0.085}$ (syst.) ± 0.041 (BR) $^{+0.854}_{-1.175}$ (extrap.)	2.52 ± 0.42
	30–50% centrality	
D^0	1.275 ± 0.099 (stat.) $^{+0.167}_{-0.173}$ (syst.) ± 0.010 (BR)	1.06 ± 0.15
D$^+$	0.552 ± 0.008 (stat.) $^{+0.024}_{-0.024}$ (syst.) ± 0.009 (BR) $^{+0.068}_{-0.114}$ (extrap.)	0.471 ± 0.069
D^{*+}	0.663 ± 0.023 (stat.) $^{+0.038}_{-0.039}$ (syst.) ± 0.007 (BR) $^{+0.149}_{-0.165}$ (extrap.)	$0.419 ^{+0.065}_{-0.061}$

drawn when the measured dN/dy of D$_s^+$, Λ_c^+, and J/ψ will be available in Pb–Pb collisions and included in the comparison, since it is expected that the modifications of the hadronisation mechanisms in the presence of a QGP affect the relative abundances of different charm-hadron species [25, 72–77].

5.2 Nuclear modification factor

The R_{AA} of prompt D^0, D$^+$, and D^{*+} mesons was computed, as defined in Eq. 1, using the d^2N/dydp_T measured in Pb–Pb collisions and the pp reference at the same centre of mass energy reported in Fig. 4. The obtained results are shown in Fig. 6 for the two centrality classes. The nuclear modification factors of the three D-meson species are compatible among each other within statistical uncertainties.

The average R_{AA} of D^0, D$^+$, and D^{*+} mesons was computed as a weighted average using the inverse of the quadratic sum of the relative statistical and uncorrelated systematic uncertainties as weights, in the p_T intervals where more than one D-meson R_{AA} value is available. The systematic uncertainties due to the raw-yield extraction and selection efficiency were considered as uncorrelated among different D-meson species and therefore they were used in the definition of the weights and propagated through the weighted average as uncorrelated, while the other sources of uncertainty (tracking efficiency, generated
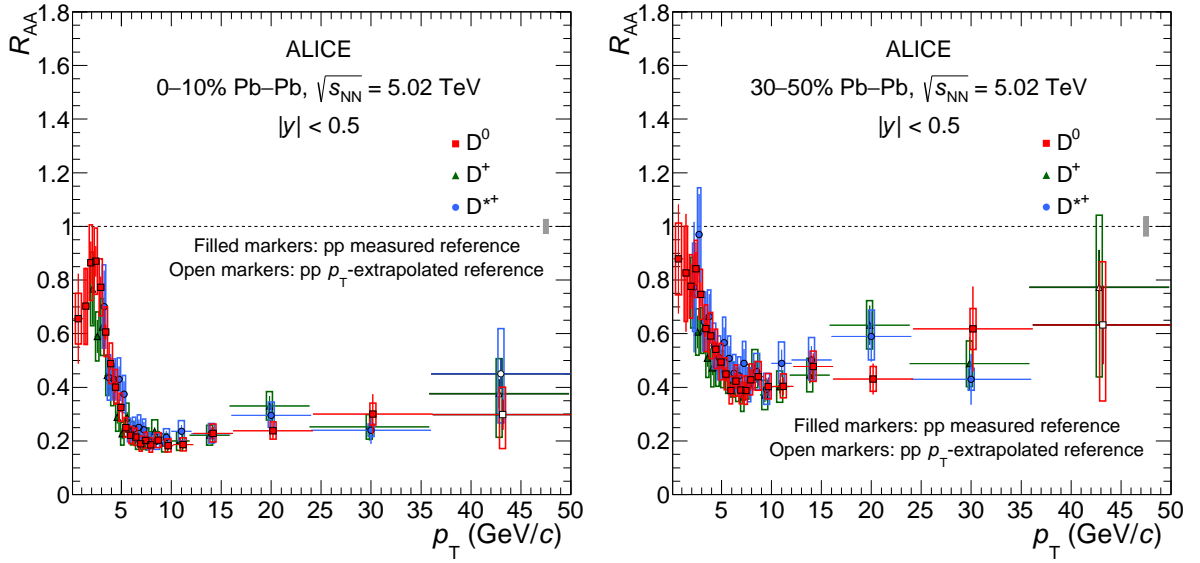
Figure 6: R_{AA} of prompt D^0, D$^+$, and D^{*+} mesons as a function of p_T for the 0–10% (left panel) and 30–50% (right panel) centrality classes. Statistical (bars), systematic (boxes), and normalisation (shaded box around unity) uncertainties are shown. Filled markers are obtained with the measured pp reference [37, 66], empty markers with the p_T-extrapolated reference.

p_T shape, and beauty hadron feed-down) were treated as fully correlated.

The prompt D-meson average nuclear modification factors in the 0–10% and 30–50% centrality classes are shown in Fig. 7 together with the R_{AA} in the 60–80% centrality class taken from Ref. [30], which was measured using the sample of Pb–Pb collisions collected in 2015. The suppression increases from peripheral to central collisions. The R_{AA} shows a minimum value at $p_T = 6$–8 GeV/c, corresponding to a suppression of the yields by a factor 5 and 2.5 with respect to the binary-scaled pp reference in the 0–10% and 30–50% classes, respectively. The stronger suppression observed in central collisions is due to the increasing medium density, size, and lifetime of the fireball from peripheral to central collisions. Also shown in Fig. 7 is the nuclear modification factor R_{pPb} measured in p–Pb collisions at $\sqrt{s_{NN}} = 5.02$ TeV taken from Ref. [33], which is compatible with unity within uncertainties, confirming that the suppression observed in Pb–Pb collisions is to due final-state effects induced by the formation of a hot and dense QGP medium.

The right panel of Fig. 7 shows the R_{AA} of prompt D mesons measured by the ALICE collaboration in Pb–Pb collisions at $\sqrt{s_{NN}} = 5.02$ TeV and 2.76 TeV [29] and of D^0 mesons measured at RHIC by the STAR collaboration in Au–Au collisions at $\sqrt{s_{NN}} = 200$ GeV [32]. The results from ALICE at the two different energies are compatible within uncertainties. This similarity originates from the interplay between the higher medium temperature and density at 5.02 TeV, which causes a larger energy loss and a lower R_{AA}, and the harder p_T distribution of charm quarks at 5.02 TeV, which would increase the R_{AA} if the medium temperature were the same at the two collision energies [63]. The nuclear modification factor of D^0 mesons at RHIC energies shows a trend with p_T similar to the one measured at the LHC, with a possible hint for a smaller R_{AA} at low p_T (< 2 GeV/c) and a larger R_{AA} at high p_T (> 4 GeV/c) in collisions at $\sqrt{s_{NN}} = 200$ GeV compared to LHC energies. This difference could be due to dependence with collision energy of the charm-quark p_T distributions, the initial-/final-state effects, and the medium properties. However, the rather large uncertainties prevent a firm conclusion on a $\sqrt{s_{NN}}$ dependence of the R_{AA} from being drawn.

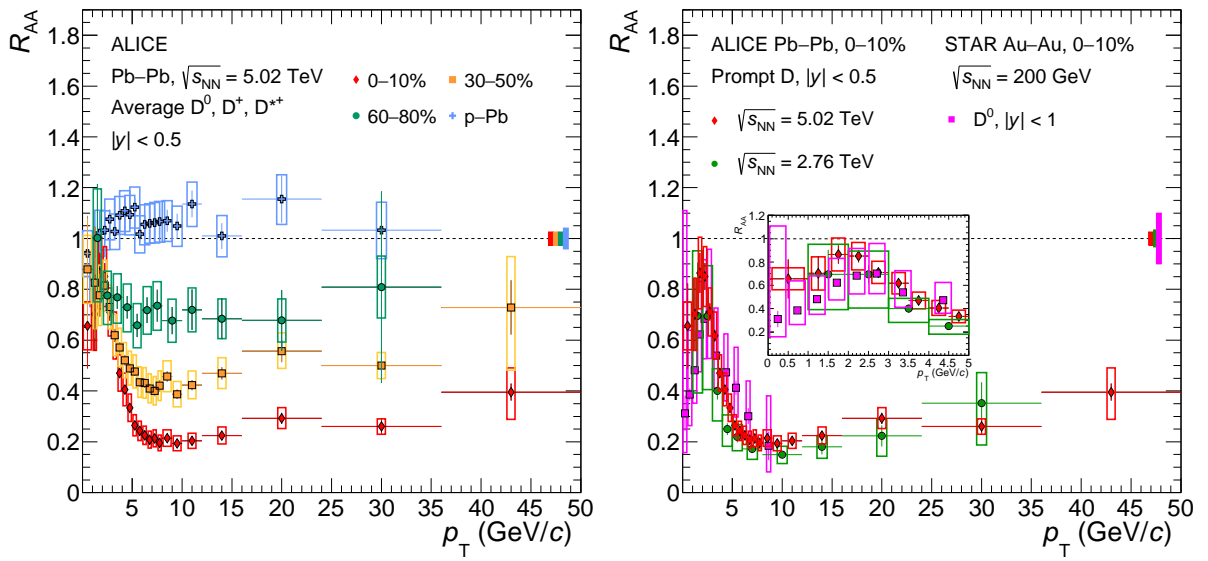In addition, the p_T-integrated R_{AA} of prompt D^0 mesons at midrapidity was calculated from the p_T-

Figure 7: Left panel: prompt D-meson R_{AA} (average of D⁰, D⁺, and D^{*+}) as a function of p_T measured in Pb–Pb collisions at $\sqrt{s_{NN}} = 5.02$ TeV (2018 data sample) in the 0–10% and 30–50% centrality classes compared with published results in the 60–80% centrality class (2015 data sample) [30] and in p–Pb collisions at the same centre-of-mass energy [33]. Statistical (bars), systematic (boxes), and normalisation (shaded box around unity) uncertainties are shown. Right panel: prompt D-meson R_{AA} in the 10% most central Pb–Pb collisions at $\sqrt{s_{NN}} = 5.02$ TeV and 2.76 TeV [29] compared to the D⁰ R_{AA} measured by the STAR collaboration in Au–Au collisions at $\sqrt{s_{NN}} = 200$ GeV [32].

integrated yield in Pb–Pb collisions reported above and the D⁰ production cross section measured in pp collisions at $\sqrt{s_{NN}} = 5.02$ TeV [37]. The results in the 0–10% and 30–50% centrality classes are:

$$R_{AA}^{\text{prompt D}^0}(0\text{–}10\%) = 0.689 \pm 0.054 \,(\text{stat.})^{+0.104}_{-0.106}\,(\text{syst.}),$$
$$R_{AA}^{\text{prompt D}^0}(30\text{–}50\%) = 0.775 \pm 0.069 \,(\text{stat.})^{+0.117}_{-0.120}\,(\text{syst.}).$$

(4)

Figure 8 shows the results obtained in Pb–Pb collisions compared with the nuclear modification factor R_{pPb} measured in p–Pb collisions at the same centre-of-mass energy [33]. The total charm cross section is expected to scale with the number of binary collisions N_{coll}, as introduced in Section 1, and thus the R_{AA} should be equal to one. However, the nuclear shadowing effect reduces the charm production in Pb–Pb (and p–Pb) collisions with respect to pp interactions. In addition, the possible enhanced production of D_s^+ and Λ_c^+ due to the hadronisation via recombination is expected to further decrease the fraction of charm quarks that hadronise into D⁰ mesons in Pb–Pb collisions compared to pp collisions [25, 72–77]. The measured p_T-integrated R_{AA} is significantly below unity and this confirms the suppression of the D⁰-meson yield in Pb–Pb collisions with respect to the binary-scaled pp reference due to shadowing and the possible modifications in the hadronisation mechanism. Conversely, the p_T-integrated D⁰ R_{pPb} is closer to unity, as expected from the smaller shadowing effects in p–Pb compared to Pb–Pb collisions (where it affects the nucleons of both the projectile and the target nuclei). The integrated R_{AA} is also compared with perturbative QCD calculations of D⁰-meson production including only initial-state effects modeled using two different sets of nuclear PDFs, namely nCTEQ15 [78–82] and EPPS16 [83, 84]. The calculations with EPPS16 do not include the dependence of the shadowing on the impact parameter of the Pb–Pb collision and therefore they are the same in the central and semicentral event classes. The predictions with nCTEQ15 are obtained applying a Bayesian reweighting of the nuclear PDFs, which is constrained by measurements of heavy-flavour production in p–Pb collisions at the LHC [79], and are labelled as nCTEQ15_{rwHF} in Fig. 8. They include a modelling of the centrality
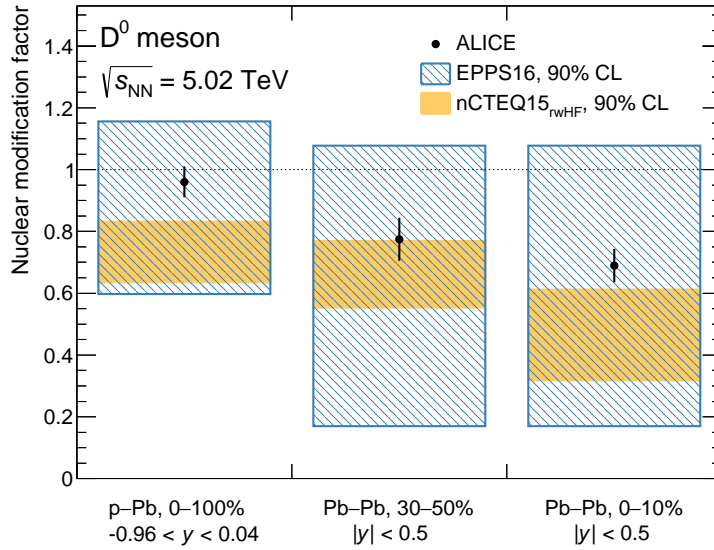
18

Figure 8: p_T-integrated nuclear modification factors of prompt D^0 mesons measured in p–Pb [33] and Pb–Pb collisions at $\sqrt{s_{NN}} = 5.02$ TeV. Statistical (bars) and systematic (brackets) uncertainties are shown. The results are compared with calculations at 90% of confidence level of theoretical models nCTEQ15 (with Bayesian reweighting, see text for details) [78–82] and EPPS16 [83, 84] that include only initial-state effects.

dependence of the nuclear modification of the PDFs. The uncertainty bands represent a 90% confidence level uncertainty. In the nCTEQ15 case they are determined by considering three different factorisation scales in addition to the PDF uncertainties, with the scale variation constituting the main source of uncertainty, as described in Ref. [79]. Both model calculations include only the initial-state effects due to the nuclear PDFs, but not the possible modifications of the relative abundances of different charm hadron species due to hadronisation via recombination. The measured R_{AA} values lie on the upper edge of the theoretical predictions and this could be due to a smaller shadowing effect in the data with respect to the model expectations.

5.3 Discussion: energy loss regime

The comparison of the nuclear modification factor of prompt D mesons with that of pions and of particles originating from beauty-hadron decays can provide essential insights into the characteristics of the in-medium parton energy loss, in particular on its predicted dependence on the colour charge and the quark mass. To investigate possible differences with respect to light-flavour particles, the average R_{AA} of prompt D^0, D^+, and D^{*+} mesons in the 0–10% centrality class is compared in Fig. 9 with that of charged pions [85] and charged particles [86]. The charged-particle R_{AA} is shown for $p_T > 20$ GeV/c in order to extend the comparison to light-flavour particles up to the highest p_T interval of the D-meson measurement. The R_{AA} of charged particles can be used in this comparison at high p_T in place of the pion one because for $p_T > 8$–10 GeV/c. In this range, the nuclear modification factors of different light-flavour hadron species are found to be consistent with each other and the particle composition is compatible with that measured in pp collisions, that is dominated by pions [85, 87].

The R_{AA} of D mesons is larger than that of pions for $p_T < 8$ GeV/c, providing a clear evidence for a different nuclear modification factor of D mesons and light-flavour particles at low and intermediate p_T. This difference originates from the interplay of several effects that concur in determining the magnitude and the p_T-dependence of the R_{AA}, so the intepretation in terms of different in-medium parton energy loss of charm quarks, light quarks, and gluons is not straighforward. As pointed out in Ref. [19], also
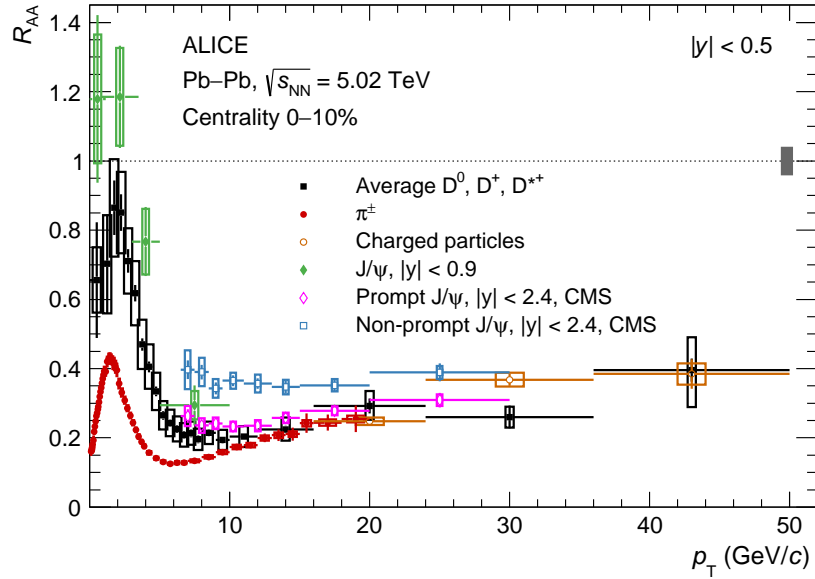
Figure 9: Average R_{AA} of prompt D^0, D^+, and D^{*+} mesons in the 0–10% centrality class compared to R_{AA} of charged pions [85], charged particles [86], inclusive J/ψ measured by ALICE [88], and of prompt and non-prompt J/ψ from CMS [61] in Pb–Pb collisions at $\sqrt{s_{NN}} = 5.02$ TeV.

in the presence of a colour-charge and quark-mass dependent energy loss, similar values of D-meson and pion R_{AA} are expected at high p_T ($\gtrsim 8$ GeV/c) due to the harder p_T distribution and the harder fragmentation function of charm quarks compared to those of light quarks and gluons. At low p_T, where a large difference is observed between the D-meson and pion R_{AA}'s, it should be considered that the pion yield can have a significant contribution from soft production up to transverse momenta of about 3–4 GeV/c due to the strong radial flow at LHC energies. This soft component, which is not present in the D-meson production, does not scale with the number of binary nucleon–nucleon collisions. In addition, effects due to the radial flow and the hadronisation can affect D-meson and light-hadron yields differently at a given p_T, playing a role in the interpretation of their different R_{AA} at low and intermediate p_T. For instance, an enhanced production of D_s^+ mesons and charm baryons in Pb–Pb collisions due to recombination would imply a reduction of the fraction of charm quarks hadronising into non-strange meson species compared to pp collisions.

A quantitative understanding of the parton in-medium energy-loss from the R_{AA} measurements needs therefore to be carried out via comparisons with model calculations. In particular, in the high-p_T region, where effects due to radial flow and modifications in the hadronisation mechanisms are expected to be negligible, models based on perturbative QCD (pQCD) calculations of high-p_T parton energy loss are expected to describe the data. The R_{AA} and the elliptic flow v_2 of prompt D mesons (taken from Ref. [36]) and pions (taken from Ref. [85,89]) in the 0–10% and 30-50% centrality classes are compared in Fig. 10 to three of these models, namely CUJET3.1 [90–92], DREENA-A [93–95], and SCET$_{M,G}$ [96]. The DREENA-A is a numerical framework that calculates the medium-modified distribution of high-p_T hadrons based on a dynamical energy-loss formalism coupled with a modelling of initial parton momentum distributions, a full 3+1D hydrodynamic evolution of the medium, and fragmentation functions. The dynamical energy-loss formalism [97–99] is a model of jet-medium interactions incorporating collisional and radiative energy loss mechanisms in a QCD medium of finite size and temperature composed of dynamical scattering centers. It includes a colour-charge and quark-mass dependence as well as finite magnetic mass effects and running strong coupling constant. The CUJET3.1 framework provides a calculation of jet energy loss in a QCD medium described with relativistic viscous hydrodynamics.
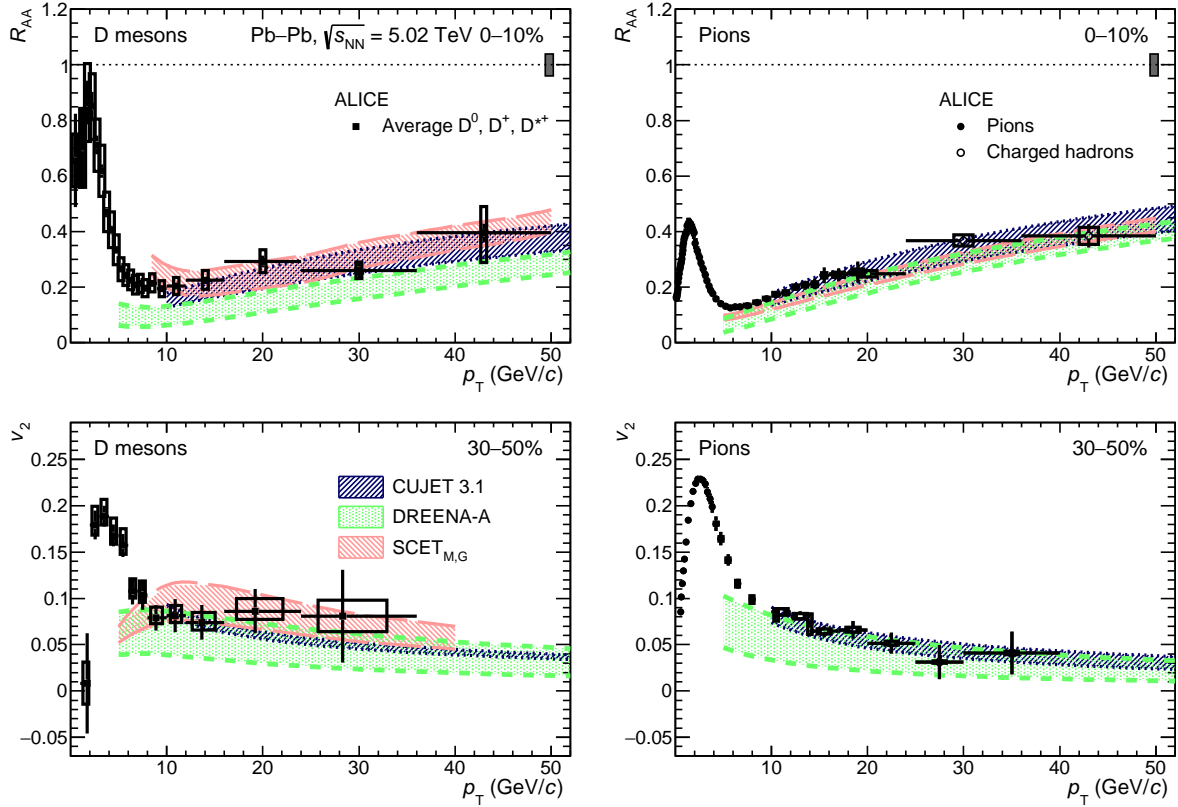
20

Figure 10: Average R_{AA} (top panels) and v_2 (bottom panels) of prompt D^0, D^+, and D^{*+} mesons [36] and pions (charged hadrons) [85, 86, 89] compared with predictions from models based on pQCD calculations, namely CUJET3.1 [90–92], DREENA-A [93], and SCET$_{M,G}$ [96].

The jet-medium interactions are based on the DGLV opacity expansion model [22, 100, 101] including both inelastic and elastic scatterings with their colour-charge and quark-mass dependence, and taking into account interactions with both chromo-electric and magnetic charges of the medium. The SCET$_{M,G}$ model implements medium-induced gluon radiation via modified splitting functions. It is based on a soft-collinear effective theory (SCET [102, 103]) describing the parton shower formed in the vacuum via soft and collinear splittings. This effective theory was extended to the case of massless [104, 105] and massive [96] quarks propagating in strongly-interacting matter by including additional splitting processes induced by the interactions of the incident parton with the QCD medium mediated by Glauber gluon exchange. These medium-induced splittings are calculated to first order in the opacity series expansion, thus limiting the applicability of these calculations to the high p_T region.

The considered models provide a fair description of both the R_{AA} and the v_2 of D mesons and pions for $p_T > 10$ GeV/c, where radiative energy loss is expected to be the dominant interaction mechanism. This suggests that the dependences of radiative energy loss on the colour charge and the quark mass of the hard-scattered parton, as well as on the path length in the hot and dense medium are reasonably well described in these calculations.

The comparison of the nuclear modification factors of particles originating from charm and beauty quarks is also reported in Fig. 9, to provide insight into the predicted quark-mass dependence of parton energy loss. In particular, the R_{AA} of inclusive J/ψ mesons measured by ALICE [88] at midrapidity and those of prompt and non-prompt J/ψ from the CMS collaboration [61] are shown.

The R_{AA} of prompt D mesons in the 0–10% centrality class is lower than that of non-prompt J/ψ mesons

from beauty hadron decays measured in the same centrality interval. This difference provides an indication for the predicted quark-mass dependence of in-medium energy loss, even though a proper interpretation of the different nuclear modification factors in terms of energy loss requires a full modelling of the initial momentum distributions of charm and beauty quarks, of the heavy-quark fragmentation, and of the beauty-hadron decay kinematics. The model from Ref. [106], which includes all these effects, provides a good description of the measurements of prompt D and non-prompt J/ψ mesons. In this model, the large difference in the R_{AA}'s in the p_T interval around 10 GeV/c is mostly due to the different in-medium energy loss of c and b quarks, as the effects of initial distributions, quark fragmentation, and beauty-hadron decays are found to be small.

The comparison of the nuclear modification factors of prompt D mesons and prompt (inclusive) J/ψ mesons, also shown in Fig. 9, provides insight into the interplay of different QGP medium effects in the charm sector, where they are expected to affect differently the production of open charm and charmonium states. At high momentum ($p_T \gtrsim 10$ GeV/c), the R_{AA} of prompt D mesons is compatible within uncertainties with that of prompt J/ψ mesons, as well as with that of light-flavour hadrons. This may suggest that in this p_T region the yield of charmonia has a significant contribution from production within the parton shower originating from the splitting of a hard-scattered gluon [107, 108], which experiences in-medium energy loss before fragmenting [109, 110]. At lower p_T ($2 \lesssim p_T \lesssim 4$ GeV/c), the results for inclusive J/ψ, which are dominated by the prompt contribution, show a magnitude and a trend of the R_{AA} similar to that of D mesons. In this region, J/ψ production is likely dominated by recombination of c and $\overline{c}$ quarks in the medium either at the phase boundary or during the QGP expansion [88, 111], similarly to the recombination of charm and light quarks forming D mesons. The similar R_{AA} of J/ψ and D mesons in this momentum region may signal the dominant contribution of hadronisation via recombination after the interactions of the charm quarks with the QGP medium constituents [112–115], with possible small differences arising from the different kinematics involved in the charm-quark coalescence with $\overline{c}$ and light antiquarks.

5.4 Discussion: transport models and an estimate of the spatial diffusion coefficient

As discussed in Section 1, the charm-hadron yields and angular distributions at low and intermediate p_T are sensitive to the diffusion and the possible thermalisation of charm quarks in the medium. The comparison of the measured D-meson R_{AA} and v_2 to models implementing charm-quark transport in a hydrodynamically expanding QGP could therefore provide insight into the interactions of heavy quarks with the medium, constraining in particular the spatial diffusion coefficient, which is the relevant transport coefficient in the diffusion regime. In the left panels of Fig. 11 the measured nuclear modification factor of prompt D mesons for the 0–10% (top) and 30–50% (bottom) centrality class, respectively, is compared with various predictions from models implementing charm-quark transport in a hydrodynamically expanding medium [77, 116–126]. In particular, the TAMU [77], POWLANG-HTL [118, 119], PHSD [126], and Catania [123, 124] models describe the interactions of the charm quarks with the medium constituents solely via collisional processes, while the MC@sHQ+EPOS2 [116], DAB-MOD [117], LBT [120, 121], LGR [122], and LIDO [125] calculations include also radiative processes. All the models, except for DAB-MOD, include initial-state effects by using nuclear PDFs (nPDFs) in the calculation of the initial p_T distributions of charm quarks. A contribution of hadronisation via quark recombination, in addition to charm-quark fragmentation, is included in all theoretical predictions. The theoretical uncertainties, where available, are displayed with a coloured band.

Most of the models capture the measured p_T trend and magnitude of the nuclear modification factor and provide a good description of the data in the p_T interval $6 < p_T < 10$ GeV/c where the minimum of the R_{AA} is observed, but many of them show significant deviations from the measurements at low p_T ($p_T \lesssim 4$–5 GeV/c). In particular, the LBT [120, 121], LIDO [125], MC@sHQ+EPOS2 [116], and Catania [123, 124] calculations tend to underestimate the results for $2 < p_T < 4$ GeV/c in both centrality classes, while the PHSD [126] prediction is above the measured R_{AA} in semicentral collisions for the
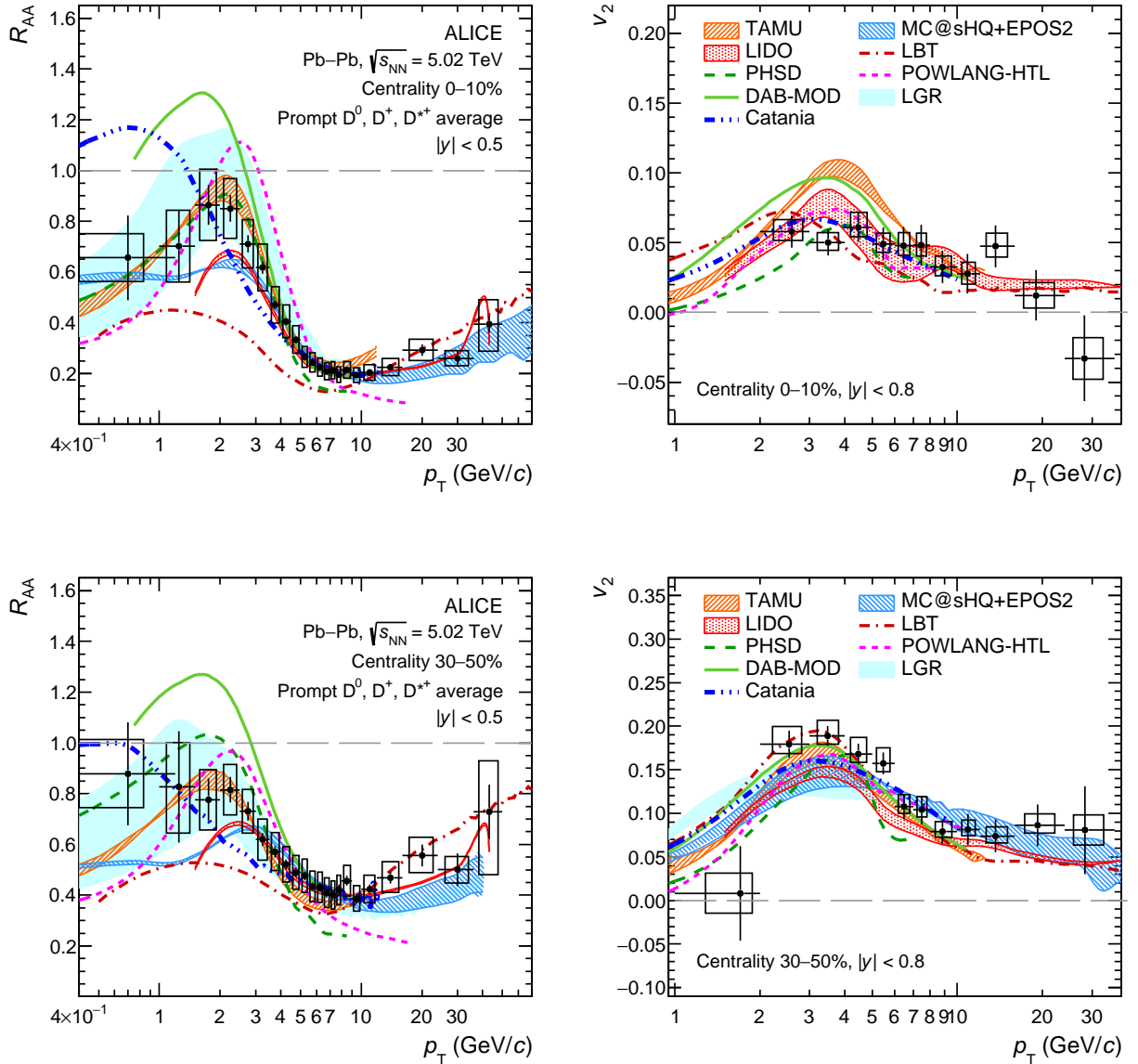
Figure 11: Average R_{AA} (left) and elliptic flow v_2 [36] (right) of prompt D^0, D$^+$, and D^{*+} mesons in the 0–10% (top) and 30–50% (bottom) centrality classes compared with predictions of models implementing the charm-quark transport in a hydrodynamically expanding medium [77, 116–126].

same p_T range. The POWLANG-HTL [118, 119] calculation, instead, predicts a narrower and more pronounced radial flow peak at low p_T as compared to the measured one for the 10% most central Pb–Pb collisions. Most of the models underestimate the measured R_{AA} in both centrality classes for $p_T < 1.5$ GeV/c, with the exception of Catania [123, 124] calculations, which tend to overpredict the measured R_{AA} at low p_T in central and semicentral collisions and PHSD predictions, which overestimate the R_{AA} in the 30–50% centrality class. Nevertheless, it is important to remark that the R_{AA} at low p_T is sensitive not only to the modelling of the charm-quark interactions with the medium but also to the parametrisation of the nPDFs used in the calculations and to the hydrodynamical description of the underlying medium.

More stringent constraints to the implementation of the heavy-quark interactions with the medium con-

stituents can be provided by the simultaneous comparison of R_{AA} and v_2 measurements in Pb–Pb collisions at $\sqrt{s_{NN}} = 5.02$ TeV [36] with models, as reported in Fig. 11. All the models describe reasonably well the v_2 in the most central collisions, while they tend to underestimate the measured points in the $2 < p_T < 6$ GeV/c interval for the 30–50% centrality class, except for LBT which reproduces well the measured v_2 but misses completely the R_{AA} in the same p_T range. In this p_T region, the measured v_2 originates predominantly from the charm-quark interactions with the QGP constituents, which impart the flow of the medium to the heavy quarks, and from the hadronisation via recombination, which enhances the charm-hadron v_2 with respect to the one of the charm quark because the D meson picks up the v_2 of the light quark. Similarly, the peak observed in the R_{AA} for $2 < p_T < 6$ GeV/c is also due to the interplay between the diffusion and recombination of the charm quarks with the medium constituents. Thus, the measurements of the R_{AA} and v_2 in this p_T region are particularly sensitive to quark diffusion and thermalisation with the medium, and to the hadronisation mechanisms.

The simultaneous description of R_{AA} and v_2 is challenging for the models and therefore the data have the potential to constrain the model ingredients and parameters. The global agreement between the measured R_{AA} and the theoretical models was evaluated by computing a χ^2/ndf, as done in Refs. [36, 127]. The statistical and systematic uncertainties (treating separately the contributions correlated and uncorrelated among p_T intervals) were considered in the calculation together with the theoretical ones, when available. Since the upper p_T limit of the predictions is different for each model, the χ^2/ndf was computed in the $0 < p_T < 8$ GeV/c interval, which is common among all the models except for the LIDO predictions which start from 1.5 GeV/c. Therefore, the χ^2/ndf computation for LIDO was performed excluding the first two p_T intervals of the R_{AA}. This low-p_T range provides high sensitivity to charm-quark diffusion and hadronisation in the QGP. The χ^2/ndf values are reported in Table 5. The large spread in the computed χ^2/ndf is not only due to the improved precision of the measurement, but also to the differences among the theoretical models. They do not only differ in terms of the interaction of charm quarks with the medium, as previously highlighted, but also in terms of the considered nuclear PDFs, the bulk evolution of the medium (i.e. ideal or viscous hydrodynamics), the charm hadronisation mechanism (i.e. fragmentation and/or recombination), and whether a hadronic phase is included or not. In particular, the charm-quark recombination mechanism is implemented with different approaches in the various models: most of the models use an instantaneous recombination based on the Wigner function formalism [128], while TAMU implements a resonance-recombination model [129], PHSD a dynamical coalescence via a Monte Carlo approach [126], and POWLANG an in-medium string formation approach [118]. The R_{AA} predictions are deeply influenced by these additional model ingredients, other than the transport properties of the medium. Therefore, a rather mild requirement on the data-to-model consistency, namely $\chi^2/\text{ndf} < 5$, was applied to select the models considered for the estimation of the heavy-quark spatial diffusion coefficient. With this criterion, the selected models are TAMU [77], MC@sHQ+EPOS2 [116], LIDO [125], LGR [122], and Catania [123, 124]. A similar analysis was performed for the elliptic and triangular flow [36]. In order to further constrain the description of heavy-quark transport in the medium and the spatial diffusion coefficient D_s, the results of the χ^2/ndf analysis for the R_{AA} model calculations were combined with those obtained for the elliptic and triangular flow in Ref. [36]. Note that some theoretical predictions for the v_2 were updated after the publication of Ref. [36], namely LBT [120, 121], LIDO [125], LGR [122], PHSD [126], and TAMU [77]. Therefore the χ^2/ndf of these predictions with respect to the measured v_2 and v_3 was re-computed. The outcome did not change significantly with respect to Ref. [36], with the only exception of LIDO [125] for which the updated predictions provide a better description of the data with respect to the old ones, resulting in a $\chi^2/\text{ndf} < 2$. Thus, the LIDO model is included among those providing a good description of v_2 and v_3, while it was not considered in Ref. [36]. The models that describe reasonably well both R_{AA} (with $\chi^2/\text{ndf} < 5$) and v_2 and v_3 (with $\chi^2/\text{ndf} < 2$) are TAMU [77], MC@sHQ+EPOS2 [116], LIDO [125], LGR [122], and Catania [123, 124]. These models use a value of heavy-quark spatial diffusion coefficient in the range $1.5 < 2\pi D_s T_c < 4.5$ at the pseudocritical temperature $T_{pc} = 155$ MeV [3]. According to lQCD calculations the $2\pi D_s T_c$ lies

Table 5: Summary of the χ^2/ndf values obtained in $0 < p_T < 8$ GeV/c for the different model predictions compared with the measured D-meson R_{AA}.

Model	χ^2/ndf R_{AA} 0–10%	30–50%	global
Catania [123, 124]	94.9/15	48.9/15	143.8/30
DAB-MOD [117]	110.2/15	123.9/15	234.1/30
LBT [120, 121]	342.6/15	69.2/15	411.8/30
LIDO [125]	31.8/13	14.5/13	46.4/26
LGR [122]	4.7/15	4.5/15	9.2/30
MC@sHQ+EPOS2 [116]	31.8/15	24.8/15	56.6/30
PHSD [126]	103.2/15	191.4/15	294.7/30
POWLANG-HTL [118, 119]	331.0/15	137.6/15	468.6/30
TAMU [77]	16.7/15	13.5/15	30.2/30

between 2 and 6 [130–132], and these results are also in agreement with the D_s range estimated from the v_2 measurements by ALICE (1.5–7 from Ref. [36]), STAR (2–12 from Ref. [133]), and PHENIX (value of ∼3 from Ref. [134]). The inclusion of the R_{AA} in the χ^2/ndf improved the constraint on the spatial diffusion coefficient with respect to the range reported in Ref. [36]. It is however important to remark that this coefficient is not the only key parameter of the models describing the heavy-quark transport in an expanding medium, but there are other ingredients (such as the parameters of the underlying hydrodynamics, the modelling of the hadronisation, the description of the interactions in the hadronic phase, amongst others, see e.g. Refs. [17, 135]) playing an important role.

A deeper insight on the impact of the different implementations of the charm-quark interaction and hadronisation in the QGP can be obtained from Figs. 12 and 13. In Fig. 12 the R_{AA} and the v_2, measured in the 0–10% and 30–50% centrality classes, respectively, are compared with two different implementations of the LIDO [125] and LGR [122] models, in order to assess the role of elastic and radiative processes in the charm-quark interactions with medium constituents. In particular, the first implementation is the standard one including both elastic and radiative processes, while the second prediction was obtained by switching off the radiative processes. At low p_T (i.e. $\lesssim$ 3–4 GeV/c), the collisional processes are expected to be the dominant interaction and this is confirmed by the similarity of the predictions for prompt D-meson R_{AA} and v_2 with (full band) and without (striped band) radiative processes. This is further supported by the agreement, in the same p_T range, between the experimental data and other theoretical models which implement only elastic processes, like TAMU [77], PHSD [126], and POWLANG-HTL [118, 119]. Radiative processes, instead, become dominant at intermediate and high p_T. This can be observed in Fig. 12 where the predictions without these processes overestimate (underestimate) the measured R_{AA} (v_2) for $p_T \gtrsim$ 5–6 GeV/c.

Similarly, Fig. 13 shows the comparison of the experimental data for R_{AA} and v_2 with two different versions of the PHSD [126], POWLANG-HTL [118, 119], and DAB-MOD [117] models, in order to investigate the effects of the hadronisation mechanism, and in particular the role of recombination. This plays a key role in the predictions for R_{AA} and v_2, since the relation between the momentum of the charm hadron and that of the parent charm quark is different for the fragmentation process, where the hadron inherits a fraction of the initial quark momentum, and the recombination, where the D-meson p_T is larger than the one of the charm quark and the charm hadron inherits also the collective flow of the light quark. In Fig. 13, the predictions are provided with (solid line) and without (dashed line) the implementation of
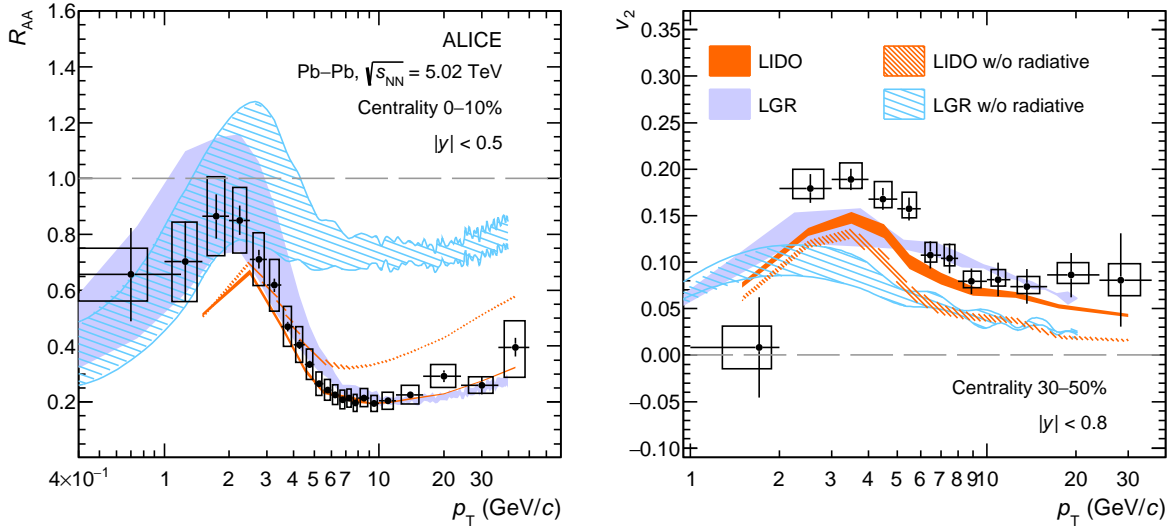
Figure 12: Prompt D-meson R_{AA} in the 0–10% centrality class (left panel) and v_2 in the 30–50% centrality class (right panel) compared with the LIDO [125] and LGR [122] predictions obtained with and without including radiative processes in the charm-quark interactions with the medium.
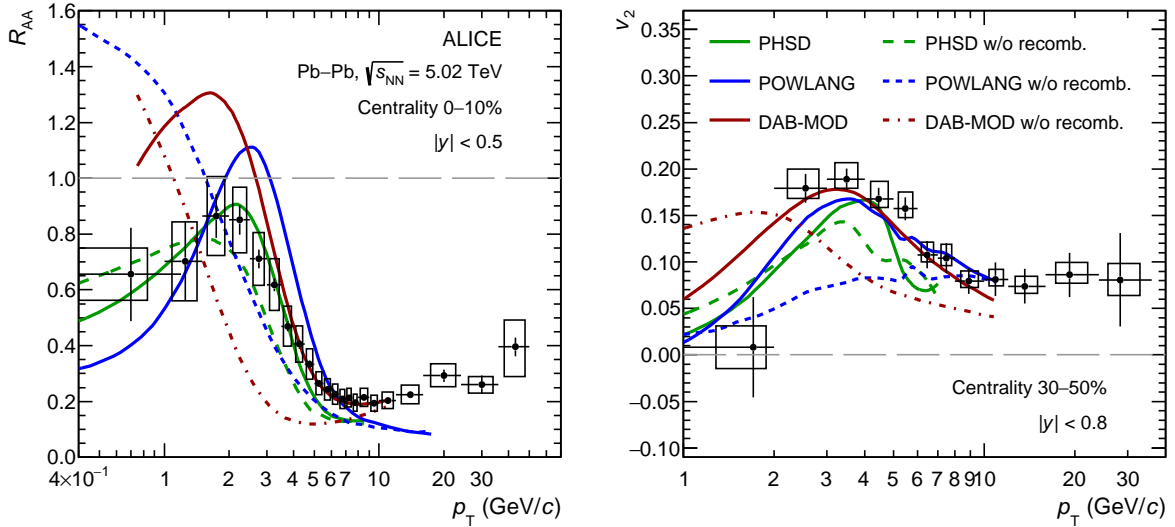

Figure 13: Prompt D-meson R_{AA} in the 0–10% centrality class (left panel) and v_2 in the 30–50% centrality class (right panel) compared with the PHSD [126], POWLANG [118, 119], and DAB-MOD [117] predictions obtained with and without including hadronisation via recombination.

the recombination process in the hadronisation mechanism. The calculations performed including only the fragmentation process underestimate both the R_{AA} and v_2, while the inclusion of the recombination of charm quarks with light quarks pushes the predictions closer to the experimental data. This indicates that recombination with light quarks from the medium plays a relevant role in the hadronisation of charm quarks at the QGP phase boundary.

6 Conclusions

We have reported the measurement of the p_T-differential production yields of prompt D^0, D^+, and D^{*+} mesons and charge conjugates at midrapidity ($|y| < 0.5$) in central and semicentral Pb–Pb collisions at a centre-of-mass energy per nucleon pair $\sqrt{s_{NN}} = 5.02$ TeV. The results were obtained with the data sample collected at the end of 2018 with the ALICE detector. The p_T-spectra were measured in finer p_T intervals with respect to the previous measurements at the same centre-of-mass energy [30], providing a more precise description of the p_T distribution. The large data sample allowed for the first measurement of the D^0-meson yield down to $p_T = 0$ in Pb–Pb collisions at the LHC. This enabled the determination of the p_T-integrated production yields of prompt D^0, which is obtained in a model independent way, of prompt D^+ and D^{*+}, and the comparison with predictions from the statistical hadronisation model [67, 68]. The average R_{AA} of the D^0, D^+, and D^{*+} mesons reaches a maximum suppression value of 5.5 (i.e. $R_{AA} \sim 0.18$) and 2.7 (i.e. $R_{AA} \sim 0.4$) in the 0–10% and 30–50% centrality classes, respectively, at $p_T = 6$–8 GeV/c. This suppression becomes less pronounced in peripheral collisions with a minimum value of 0.7–0.8, as observed in the 60–80% centrality class in Ref. [30], and it is due to final-state effects, since it is not observed in minimum bias p–Pb collisions [33]. However, it was pointed out in Ref. [136, 137] that event selection and geometry biases can cause an apparent suppression of R_{AA}, especially in peripheral collisions, even in the absence of nuclear effect. The R_{AA} of prompt D mesons at $p_T > 8$ GeV/c is well described by models which include both collisional and radiative energy loss processes. In addition, the p_T-integrated R_{AA} of prompt D^0 mesons was obtained and compared with the R_{pPb} measured in p–Pb collisions at the same centre-of-mass energy [33]. The results lie on the upper edge of the calculations which consider nuclear modification of the PDFs.

In central collisions, the p_T-differential R_{AA} of prompt D mesons is compatible within uncertainties with that of charged particles for $p_T \gtrsim 8$ GeV/c and prompt J/ψ mesons for $p_T \gtrsim 10$ GeV/c, while an ordering in R_{AA} is observed at lower p_T. The latter is due to the interplay of different effects, such as the diffusion of charm quarks in the medium possibly leading to their thermalisation in the QGP and the hadronisation via recombination with light quarks from the medium, which along with energy loss contribute to the modification of the p_T-distribution of the hadrons. The comparison of the R_{AA} of prompt D mesons and non-prompt J/ψ for $p_T > 6$ GeV/c together with model calculations supports the predictions of quark-mass dependent energy loss. At low and intermediate p_T ($\lesssim 6$–8 GeV/c), the R_{AA} is well described by different transport model calculations for the two centrality classes. However, most of them fail in describing simultaneously both R_{AA} and v_2 in central and semicentral Pb–Pb collisions. By considering the few models that are in fair agreement with both observables, the heavy-quark spatial diffusion coefficient was estimated to be in the range $1.5 < 2\pi D_s T_c < 4.5$ at the pseudocritical temperature $T_{pc} = 155$ MeV, which is a narrower interval as compared to estimations based on previous D-meson measurements at LHC energies [36, 138]. Therefore, the simultaneous comparison of the data with the theoretical predictions for these observables allowed for more stringent constraints to the heavy-quark spatial diffusion coefficient and for significant progress in the understanding of the interaction processes and the hadronisation mechanisms of charm quarks in the high-density QCD medium.

References

[1] J. C. Collins and M. J. Perry, "Superdense matter: Neutrons or asymptotically free quarks?", *Phys. Rev. Lett.* **34** (1975) 1353–1356.

[2] F. Karsch, "Lattice simulations of the thermodynamics of strongly interacting elementary particles and the exploration of new phases of matter in relativistic heavy ion collisions", *J. Phys. Conf. Ser.* **46** (2006) 122–131, arXiv:hep-lat/0608003 [hep-lat].

[3] **Wuppertal-Budapest** Collaboration, S. Borsanyi *et al.*, "Is there still any T_c mystery in lattice

QCD? Results with physical masses in the continuum limit III", *JHEP* **1009** (2010) 073, arXiv:1005.3508 [hep-lat].

[4] S. Borsanyi, Z. Fodor, C. Hoelbling, S. D. Katz, S. Krieg, and K. K. Szabo, "Full result for the QCD equation of state with 2+1 flavors", *Phys. Lett.* **B730** (2014) 99–104, arXiv:1309.5258 [hep-lat].

[5] A. Bazavov, T. Bhattacharya, M. Cheng, C. DeTar, H. Ding, *et al.*, "The chiral and deconfinement aspects of the QCD transition", *Phys. Rev.* **D85** (2012) 054503, arXiv:1111.1710 [hep-lat].

[6] W. Busza, K. Rajagopal, and W. van der Schee, "Heavy Ion Collisions: The Big Picture, and the Big Questions", *Ann. Rev. Nucl. Part. Sci.* **68** (2018) 339–376, arXiv:1802.04801 [hep-ph].

[7] **ALICE** Collaboration, K. Aamodt *et al.*, "Two-pion Bose-Einstein correlations in central Pb-Pb collisions at $\sqrt{s_{NN}} = 2.76$ TeV", *Phys. Lett.* **B696** (2011) 328–337, arXiv:1012.4035 [nucl-ex].

[8] A. Andronic *et al.*, "Heavy-flavour and quarkonium production in the LHC era: from proton-proton to heavy-ion collisions", *Eur. Phys. J.* **C76** no. 3, (2016) 107, arXiv:1506.03981 [nucl-ex].

[9] F.-M. Liu and S.-X. Liu, "Quark-gluon plasma formation time and direct photons from heavy ion collisions", *Phys. Rev.* **C89** no. 3, (2014) 034906, arXiv:1212.6587 [nucl-th].

[10] M. H. Thoma and M. Gyulassy, "Quark damping and energy loss in the high temperature QCD", *Nucl. Phys* **B351** (1991) 491–506.

[11] E. Braaten and M. H. Thoma, "Energy loss of a heavy fermion in a hot plasma", *Phys. Rev.* **D44** (1991) 1298–1310.

[12] E. Braaten and M. H. Thoma, "Energy loss of a heavy quark in the quark - gluon plasma", *Phys. Rev.* **D44** (1991) 2625–2630.

[13] R. Baier, Y. L. Dokshitzer, A. H. Mueller, S. Peigne, and D. Schiff, "Radiative energy loss and p(T) broadening of high-energy partons in nuclei", *Nucl. Phys.* **B484** (1997) 265–282, arXiv:hep-ph/9608322 [hep-ph].

[14] M. Gyulassy and M. Plumer, "Jet quenching in dense matter", *Phys. Lett.* **B243** (1990) 432–438.

[15] S. Batsouli, S. Kelly, M. Gyulassy, and J. L. Nagle, "Does the charm flow at RHIC?", *Phys. Lett.* **B557** (2003) 26–32, arXiv:nucl-th/0212068 [nucl-th].

[16] V. Greco, C. M. Ko, and R. Rapp, "Quark coalescence for charmed mesons in ultrarelativistic heavy ion collisions", *Phys. Lett.* **B595** (2004) 202–208, arXiv:nucl-th/0312100 [nucl-th].

[17] A. Beraudo *et al.*, "Extraction of heavy-flavor transport coefficients in QCD matter", *Nucl. Phys.* **A979** (2018) 21–86, arXiv:1803.03824 [nucl-th].

[18] F. Prino and R. Rapp, "Open heavy flavor in QCD matter and in nuclear collisions", *J. Phys.* **G43** no. 9, (2016) 093002, arXiv:1603.00529 [nucl-ex].

[19] M. Djordjevic, "Heavy flavor puzzle at LHC: a serendipitous interplay of jet suppression and fragmentation", *Phys. Rev. Lett.* **112** no. 4, (2014) 042302, arXiv:1307.4702 [nucl-th].

[20] Y. L. Dokshitzer and D. Kharzeev, "Heavy quark colorimetry of QCD matter", *Phys. Lett.* **B519** (2001) 199–206, arXiv:hep-ph/0106202 [hep-ph].

[21] N. Armesto, C. A. Salgado, and U. A. Wiedemann, "Medium induced gluon radiation off massive quarks fills the dead cone", *Phys. Rev.* **D69** (2004) 114003, arXiv:hep-ph/0312106 [hep-ph].

[22] M. Djordjevic and M. Gyulassy, "Heavy quark radiative energy loss in QCD matter", *Nucl. Phys* **A733** (2004) 265–298, arXiv:nucl-th/0310076 [nucl-th].

[23] B.-W. Zhang, E. Wang, and X.-N. Wang, "Heavy quark energy loss in nuclear medium", *Phys. Rev. Lett.* **93** (2004) 072301, arXiv:nucl-th/0309040 [nucl-th].

[24] H. van Hees, V. Greco, and R. Rapp, "Heavy-quark probes of the quark-gluon plasma at RHIC", *Phys. Rev.* **C73** (2006) 034913, `arXiv:nucl-th/0508055 [nucl-th]`.

[25] A. Andronic, P. Braun-Munzinger, K. Redlich, and J. Stachel, "Statistical hadronization of charm in heavy-ion collisions at SPS, RHIC and LHC", *Phys. Lett.* **B571** (2003) 36–44, `arXiv:nucl-th/0303036 [nucl-th]`.

[26] R. Glauber and G. Matthiae, "High-energy scattering of protons by nuclei", *Nucl. Phys* **B21** (1970) 135–157.

[27] M. L. Miller, K. Reygers, S. J. Sanders, and P. Steinberg, "Glauber modeling in high energy nuclear collisions", *Ann.Rev.Nucl.Part.Sci.* **57** (2007) 205–243, `arXiv:nucl-ex/0701025 [nucl-ex]`.

[28] C. Loizides, J. Nagle, and P. Steinberg, "Improved version of the PHOBOS Glauber Monte Carlo", *SoftwareX* **1-2** (2015) 13–18, `arXiv:1408.2549 [nucl-ex]`.

[29] **ALICE** Collaboration, J. Adam *et al.*, "Transverse momentum dependence of D-meson production in Pb-Pb collisions at $\sqrt{s_{NN}}$ = 2.76 TeV", *JHEP* **03** (2016) 081, `arXiv:1509.06888 [nucl-ex]`.

[30] **ALICE** Collaboration, S. Acharya *et al.*, "Measurement of D^0, D$^+$, D^{*+} and D$_s^+$ production in Pb-Pb collisions at $\sqrt{s_{NN}}$ = 5.02 TeV", *JHEP* **10** (2018) 174, `arXiv:1804.09083 [nucl-ex]`.

[31] **CMS** Collaboration, A. M. Sirunyan *et al.*, "Nuclear modification factor of D^0 mesons in PbPb collisions at $\sqrt{s_{NN}}$ = 5.02 TeV", *Phys. Lett.* **B782** (2018) 474–496, `arXiv:1708.04962 [nucl-ex]`.

[32] **STAR** Collaboration, J. Adam *et al.*, "Centrality and transverse momentum dependence of D^0-meson production at mid-rapidity in Au+Au collisions at $\sqrt{s_{NN}}$ = 200 GeV", *Phys. Rev.* **C99** no. 3, (2019) 034908, `arXiv:1812.10224 [nucl-ex]`.

[33] **ALICE** Collaboration, S. Acharya *et al.*, "Measurement of prompt D^0, D$^+$, D^{*+}, and D$_S^+$ production in p–Pb collisions at $\sqrt{s_{NN}}$ = 5.02 TeV", *JHEP* **12** (2019) 092, `arXiv:1906.03425 [nucl-ex]`.

[34] S. Voloshin and Y. Zhang, "Flow study in relativistic nuclear collisions by Fourier expansion of Azimuthal particle distributions", *Z. Phys. C* **70** (1996) 665–672, `arXiv:hep-ph/9407282`.

[35] A. M. Poskanzer and S. A. Voloshin, "Methods for analyzing anisotropic flow in relativistic nuclear collisions", *Phys. Rev.* **C58** (1998) 1671–1678, `arXiv:nucl-ex/9805001`.

[36] **ALICE** Collaboration, S. Acharya *et al.*, "Transverse-momentum and event-shape dependence of D-meson flow harmonics in Pb-Pb collisions at $\sqrt{s_{NN}}$ = 5.02 TeV", *Phys. Lett.* **B813** (2021) 136054, `arXiv:2005.11131 [nucl-ex]`.

[37] **ALICE** Collaboration, S. Acharya *et al.*, "Measurement of D^0 , D$^+$, D^{*+} and D$_s^+$ production in pp collisions at $\sqrt{s}$ = 5.02 TeV with ALICE", *Eur. Phys. J. C* **79** no. 5, (2019) 388, `arXiv:1901.07979 [nucl-ex]`.

[38] G. D. Moore and D. Teaney, "How much do heavy quarks thermalize in a heavy ion collision?", *Phys. Rev.* **C71** (2005) 064904, `arXiv:hep-ph/0412346`.

[39] **ALICE** Collaboration, K. Aamodt *et al.*, "The ALICE experiment at the CERN LHC", *JINST* **3** (2008) S08002.

[40] **ALICE** Collaboration, B. Abelev *et al.*, "Performance of the ALICE Experiment at the CERN LHC", *Int.J.Mod.Phys.* **A29** (2014) 1430044, `arXiv:1402.4476 [nucl-ex]`.

[41] **ALICE** Collaboration, K. Aamodt *et al.*, "Alignment of the ALICE Inner Tracking System with cosmic-ray tracks", *JINST* **5** (2010) P03003, `arXiv:1001.0502 [physics.ins-det]`.

[42] J. Alme *et al.*, "The ALICE TPC, a large 3-dimensional tracking device with fast readout for ultra-high multiplicity events", *Nucl. Instrum. Methods A* **622** no. 1, (2010) 316 – 367.

[43] A. Akindinov *et al.*, "Performance of the ALICE Time-Of-Flight detector at the LHC",

Eur. Phys. J. Plus **128** (2013) 44.

[44] **ALICE** Collaboration, E. Abbas *et al.*, "Performance of the ALICE VZERO system",
JINST **8** (2013) P10016, arXiv:1306.3130 [nucl-ex].

[45] R. Arnaldi *et al.*, "The zero degree calorimeters for the ALICE experiment",
Nucl. Instrum. Meth. A **581** (2007) 397–401. [Erratum: Nucl.Instrum.Meth.A 604, 765 (2009)].

[46] **ALICE** Collaboration, J. Adam *et al.*, "Centrality dependence of the charged-particle
multiplicity density at midrapidity in Pb-Pb collisions at $\sqrt{s_{NN}}$ = 5.02 TeV",
Phys. Rev. Lett. **116** no. 22, (2016) 222302, arXiv:1512.06104 [nucl-ex].

[47] **ALICE** Collaboration, "Centrality determination in heavy ion collisions",
ALICE-PUBLIC-2018-011 (2018) .

[48] C. Loizides, J. Kamin, and D. d'Enterria, "Improved Monte Carlo Glauber predictions at present
and future nuclear colliders", *Phys. Rev.* **C97** no. 5, (2018) 054910,
arXiv:1710.07098 [nucl-ex]. [Erratum: Phys. Rev. C 99, 019901 (2019)].

[49] **Particle Data Group** Collaboration, P. Zyla *et al.*, "Review of Particle Physics",
PTEP **2020** no. 8, (2020) 083C01.

[50] **ALICE** Collaboration, J. Adam *et al.*, "Measurement of D_s^+ production and nuclear modification
factor in Pb-Pb collisions at $\sqrt{s_{NN}} = 2.76$ TeV", *JHEP* **03** (2016) 082,
arXiv:1509.07287 [nucl-ex].

[51] **ALICE** Collaboration, S. Acharya *et al.*, "Measurement of D-meson production at mid-rapidity
in pp collisions at $\sqrt{s} = 7$ TeV", *Eur. Phys. J. C* **77** no. 8, (2017) 550,
arXiv:1702.00766 [hep-ex].

[52] **ALICE** Collaboration, J. Adam *et al.*, "D-meson production in p-Pb collisions at $\sqrt{s_{NN}} = 5.02$
TeV and in pp collisions at $\sqrt{s} = 7$ TeV", *Phys. Rev.* **C94** no. 5, (2016) 054908,
arXiv:1605.07569 [nucl-ex].

[53] M. Cacciari, M. Greco, and P. Nason, "The p_T spectrum in heavy flavor hadroproduction",
JHEP **9805** (1998) 007, arXiv:hep-ph/9803400 [hep-ph].

[54] M. Cacciari, S. Frixione, and P. Nason, "The p_T spectrum in heavy flavor photoproduction",
JHEP **0103** (2001) 006, arXiv:hep-ph/0102134 [hep-ph].

[55] T. Sjöstrand *et al.*, "An introduction to PYTHIA 8.2",
Comput. Phys. Commun. **191** (2015) 159–177, arXiv:1410.3012 [hep-ph].

[56] R. Brun, F. Bruyant, F. Carminati, S. Giani, M. Maire, A. McPherson, G. Patrick, and L. Urban,
GEANT: Detector Description and Simulation Tool; Oct 1994. CERN Program Library. CERN,
Geneva, 1993. Long Writeup W5013.

[57] X. N. Wang and M. Gyulassy, "HIJING: A Monte Carlo model for multiple jet production in pp,
pA and AA collisions", *Phys. Rev.* **D44** (1991) 3501–3516.

[58] P. Skands, S. Carrazza, and J. Rojo, "Tuning PYTHIA 8.1: the Monash 2013 Tune",
Eur. Phys. J. C **74** no. 8, (2014) 3024, arXiv:1404.5630 [hep-ph].

[59] **ALICE** Collaboration, B. Abelev *et al.*, "Suppression of high transverse momentum D mesons in
central Pb-Pb collisions at $\sqrt{s_{NN}} = 2.76$ TeV", *JHEP* **1209** (2012) 112,
arXiv:1203.2160 [nucl-ex].

[60] M. Cacciari, S. Frixione, N. Houdeau, M. L. Mangano, P. Nason, *et al.*, "Theoretical predictions
for charm and bottom production at the LHC", *JHEP* **1210** (2012) 137,
arXiv:1205.6344 [hep-ph].

[61] **CMS** Collaboration, A. M. Sirunyan *et al.*, "Measurement of prompt and nonprompt
charmonium suppression in PbPb collisions at 5.02 TeV", *Eur. Phys. J. C* **78** no. 6, (2018) 509,
arXiv:1712.08959 [nucl-ex].

[62] **ATLAS** Collaboration, M. Aaboud *et al.*, "Prompt and non-prompt J/ψ and $\psi(2S)$ suppression

at high transverse momentum in 5.02 TeV Pb+Pb collisions with the ATLAS experiment", *Eur. Phys. J. C* **78** no. 9, (2018) 762, `arXiv:1805.04077 [nucl-ex]`.

[63] M. Djordjevic and M. Djordjevic, "Predictions of heavy-flavor suppression at 5.1 TeV Pb+Pb collisions at the CERN Large Hadron Collider", *Phys. Rev.* **C92** no. 2, (2015) 024918, `arXiv:1505.04316 [nucl-th]`.

[64] M. He, R. J. Fries, and R. Rapp, "Heavy flavor at the Large Hadron Collider in a strong coupling approach", *Phys. Lett.* **B735** (2014) 445–450, `arXiv:1401.3817 [nucl-th]`.

[65] **ALICE** Collaboration, J. Adam *et al.*, "Transverse momentum dependence of D-meson production in Pb-Pb collisions at $\sqrt{s_{NN}} = 2.76$ TeV", *JHEP* **03** (2016) 081, `arXiv:1509.06888 [nucl-ex]`.

[66] **ALICE** Collaboration, S. Acharya *et al.*, "Measurement of beauty and charm production in pp collisions at $\sqrt{s} = 5.02$ TeV via non-prompt and prompt D mesons", *JHEP* **05** (2, 2021) 220, `arXiv:2102.13601 [nucl-ex]`.

[67] A. Andronic, P. Braun-Munzinger, M. K. Köhler, K. Redlich, and J. Stachel, "Transverse momentum distributions of charmonium states with the statistical hadronization model", *Phys. Lett.* **B797** (2019) 134836, `arXiv:1901.09200 [nucl-th]`.

[68] A. Andronic, P. Braun-Munzinger, M. K. Köhler, A. Mazeliauskas, K. Redlich, J. Stachel, and V. Vislavicius, "The multiple-charm hierarchy in the statistical hadronization model", *JHEP* **07** (2021) 035, `arXiv:2104.12754 [hep-ph]`.

[69] A. Mazeliauskas, S. Floerchinger, E. Grossi, and D. Teaney, "Fast resonance decays in nuclear collisions", *Eur. Phys. J. C* **79** no. 3, (2019) 284, `arXiv:1809.11049 [nucl-th]`.

[70] A. Andronic, P. Braun-Munzinger, K. Redlich, and J. Stachel, "Decoding the phase structure of QCD via particle production at high energy", *Nature* **561** no. 7723, (2018) 321–330, `arXiv:1710.09425 [nucl-th]`.

[71] **ALICE** Collaboration, S. Acharya *et al.*, "Charm-quark fragmentation fractions and production cross section at midrapidity in pp collisions at the LHC", `arXiv:2105.06335 [nucl-ex]`.

[72] I. Kuznetsova and J. Rafelski, "Heavy flavor hadrons in statistical hadronization of strangeness-rich QGP", *Eur. Phys. J. C* **51** (2007) 113–133, `arXiv:hep-ph/0607203`.

[73] P. R. Sorensen and X. Dong, "Suppression of non-photonic electrons from enhancement of charm baryons in heavy ion collisions", *Phys. Rev.* **C74** (2006) 024902, `arXiv:nucl-th/0512042`.

[74] S. H. Lee, K. Ohnishi, S. Yasui, I.-K. Yoo, and C.-M. Ko, "Λ_c enhancement from strongly coupled quark-gluon plasma", *Phys. Rev. Lett.* **100** (2008) 222301, `arXiv:0709.3637 [nucl-th]`.

[75] Y. Oh, C. M. Ko, S. H. Lee, and S. Yasui, "Heavy baryon/meson ratios in relativistic heavy ion collisions", *Phys. Rev.* **C79** (2009) 044905, `arXiv:0901.1382 [nucl-th]`.

[76] M. He, R. J. Fries, and R. Rapp, "D_s-meson as quantitative probe of diffusion and hadronization in nuclear collisions", *Phys. Rev. Lett.* **110** no. 11, (2013) 112301, `arXiv:1204.4442 [nucl-th]`.

[77] M. He and R. Rapp, "Hadronization and charm-hadron ratios in heavy-ion collisions", *Phys. Rev. Lett.* **124** no. 4, (2020) 042301, `arXiv:1905.09216 [nucl-th]`.

[78] J. P. Lansberg and H. S. Shao, "Towards an automated tool to evaluate the impact of the nuclear modification of the gluon density on quarkonium, D and B meson production in proton–nucleus collisions", *Eur. Phys. J. C* **77** no. 1, (2017) 1, `arXiv:1610.05382 [hep-ph]`.

[79] A. Kusina, J. P. Lansberg, I. Schienbein, and H. S. Shao, "Gluon shadowing in heavy-flavor production at the LHC", *Phys. Rev. Lett.* **121** no. 5, (2018) 052004, `arXiv:1712.07024 [hep-ph]`.

[80] A. Kusina, J. P. Lansberg, I. Schienbein, and H. S. Shao, "Reweighted nuclear PDFs using

heavy-flavor production data at the LHC: $nCTEQ15_{rwHF}$ & $EPPS16_{rwHF}$",
Phys. Rev. **D104** no. 1, (2021) 014010, `arXiv:2012.11462 [hep-ph]`.

[81] H. S. Shao, "HELAC-Onia: An automatic matrix element generator for heavy quarkonium physics", *Comput. Phys. Commun.* **184** (2013) 2562–2570, `arXiv:1212.5293 [hep-ph]`.

[82] H. S. Shao, "HELAC-Onia 2.0: an upgraded matrix-element and event generator for heavy quarkonium physics", *Comput. Phys. Commun.* **198** (2016) 238–259, `arXiv:1507.03435 [hep-ph]`.

[83] K. Eskola, H. Paukkunen, and C. Salgado, "EPS09: A new generation of NLO and LO nuclear parton distribution functions", *JHEP* **0904** (2009) 065, `arXiv:0902.4154 [hep-ph]`.

[84] K. J. Eskola, P. Paakkinen, H. Paukkunen, and C. A. Salgado, "EPPS16: Nuclear parton distributions with LHC data", *Eur. Phys. J. C* **77** no. 3, (2017) 163, `arXiv:1612.05741 [hep-ph]`.

[85] **ALICE** Collaboration, S. Acharya *et al.*, "Production of charged pions, kaons, and (anti-)protons in Pb-Pb and inelastic pp collisions at $\sqrt{s_{NN}}$ = 5.02 TeV", *Phys. Rev.* **C101** no. 4, (2020) 044907, `arXiv:1910.07678 [nucl-ex]`.

[86] **ALICE** Collaboration, S. Acharya *et al.*, "Transverse momentum spectra and nuclear modification factors of charged particles in pp, p–Pb and Pb–Pb collisions at the LHC", *JHEP* **11** (2018) 013, `arXiv:1802.09145 [nucl-ex]`.

[87] **ALICE** Collaboration, B. Abelev *et al.*, "Production of charged pions, kaons and protons at large transverse momenta in pp and Pb–Pb collisions at $\sqrt{s_{NN}}$ =2.76 TeV", *Phys. Lett.* **B736** (2014) 196–207, `arXiv:1401.1250 [nucl-ex]`.

[88] **ALICE** Collaboration, S. Acharya *et al.*, "Centrality and transverse momentum dependence of inclusive J/ψ production at midrapidity in Pb-Pb collisions at $\sqrt{s_{NN}}$ = 5.02 TeV", *Phys. Lett.* **B805** (2020) 135434, `arXiv:1910.14404 [nucl-ex]`.

[89] **ALICE** Collaboration, S. Acharya *et al.*, "Anisotropic flow of identified particles in Pb-Pb collisions at $\sqrt{s_{NN}}$ = 5.02 TeV", *JHEP* **09** (2018) 006, `arXiv:1805.04390 [nucl-ex]`.

[90] J. Xu, J. Liao, and M. Gyulassy, "Consistency of perfect fluidity and jet quenching in semi-quark-gluon monopole plasmas", *Chin. Phys. Lett.* **32** no. 9, (2015) 092501, `arXiv:1411.3673 [hep-ph]`.

[91] J. Xu, J. Liao, and M. Gyulassy, "Bridging soft-hard transport properties of quark-gluon plasmas with CUJET3.0", *JHEP* **02** (2016) 169, `arXiv:1508.00552 [hep-ph]`.

[92] S. Shi, J. Liao, and M. Gyulassy, "Global constraints from RHIC and LHC on transport properties of QCD fluids in CUJET/CIBJET framework", *Chin. Phys. C* **43** no. 4, (2019) 044101, `arXiv:1808.05461 [hep-ph]`.

[93] S. Stojku, B. Ilic, M. Djordjevic, and M. Djordjevic, "Extracting the temperature dependence in high-$p_\perp$ particle energy loss", *Phys. Rev.* **C103** no. 2, (2021) 024908, `arXiv:2007.07851 [nucl-th]`.

[94] D. Zigic, I. Salom, J. Auvinen, M. Djordjevic, and M. Djordjevic, "DREENA-B framework: first predictions of R_{AA} and v_2 within dynamical energy loss formalism in evolving QCD medium", *Phys. Lett.* **B791** (2019) 236–241, `arXiv:1805.04786 [nucl-th]`.

[95] D. Zigic, I. Salom, J. Auvinen, M. Djordjevic, and M. Djordjevic, "DREENA-C framework: joint R_{AA} and v_2 predictions and implications to QGP tomography", *J. Phys. G* **46** no. 8, (2019) 085101, `arXiv:1805.03494 [nucl-th]`.

[96] Z.-B. Kang, F. Ringer, and I. Vitev, "Effective field theory approach to open heavy flavor production in heavy-ion collisions", *JHEP* **03** (2017) 146, `arXiv:1610.02043 [hep-ph]`.

[97] M. Djordjevic, "Theoretical formalism of radiative jet energy loss in a finite size dynamical QCD medium", *Phys. Rev.* **C80** (2009) 064909, `arXiv:0903.4591 [nucl-th]`.

[98]   M. Djordjevic and U. W. Heinz, "Radiative energy loss in a finite dynamical QCD medium",
       Phys. Rev. Lett. **101** (2008) 022302, `arXiv:0802.1230 [nucl-th]`.

[99]   M. Djordjevic, "Collisional energy loss in a finite size QCD matter",
       Phys. Rev. **C74** (2006) 064907, `arXiv:nucl-th/0603066`.

[100] M. Gyulassy, P. Levai, and I. Vitev, "Non-abelian energy loss at finite opacity",
       Phys. Rev. Lett. **85** (2000) 5535–5538, `arXiv:nucl-th/0005032`.

[101] M. Gyulassy, P. Levai, and I. Vitev, "Reaction operator approach to non-abelian energy loss",
       Nucl. Phys. **B594** (2001) 371–419, `arXiv:nucl-th/0006010`.

[102] C. W. Bauer, S. Fleming, D. Pirjol, and I. W. Stewart, "An effective field theory for collinear and
       soft gluons: Heavy to light decays", *Phys. Rev.* **D63** (2001) 114020, `arXiv:hep-ph/0011336`.

[103] C. W. Bauer, D. Pirjol, and I. W. Stewart, "Soft collinear factorization in effective field theory",
       Phys. Rev. **D65** (2002) 054022, `arXiv:hep-ph/0109045`.

[104] A. Idilbi and A. Majumder, "Extending soft-collinear-effective-theory to describe hard jets in
       dense QCD media", *Phys. Rev.* **D80** (2009) 054022, `arXiv:0808.1087 [hep-ph]`.

[105] G. Ovanesyan and I. Vitev, "An effective theory for jet propagation in dense QCD matter: jet
       broadening and medium-induced bremsstrahlung", *JHEP* **06** (2011) 080,
       `arXiv:1103.1074 [hep-ph]`.

[106] M. Djordjevic, B. Blagojevic, and L. Zivkovic, "Mass tomography at different momentum ranges
       in quark-gluon plasma", *Phys. Rev.* **C94** no. 4, (2016) 044908, `arXiv:1601.07852 [nucl-th]`.

[107] **LHCb** Collaboration, R. Aaij *et al.*, "Study of J/ψ Production in Jets",
       Phys. Rev. Lett. **118** no. 19, (2017) 192001, `arXiv:1701.05116 [hep-ex]`.

[108] R. Bain, L. Dai, A. Leibovich, Y. Makris, and T. Mehen, "NRQCD confronts LHCb data on
       quarkonium production within jets", *Phys. Rev. Lett.* **119** no. 3, (2017) 032002,
       `arXiv:1702.05525 [hep-ph]`.

[109] M. Spousta, "On similarity of jet quenching and charmonia suppression",
       Phys. Lett. **B767** (2017) 10–15, `arXiv:1606.00903 [hep-ph]`.

[110] F. Arleo, "Quenching of hadron spectra in heavy ion collisions at the LHC",
       Phys. Rev. Lett. **119** no. 6, (2017) 062302, `arXiv:1703.10852 [hep-ph]`.

[111] **ALICE** Collaboration, J. Adam *et al.*, "Differential studies of inclusive J/ψ and ψ(2S)
       production at forward rapidity in Pb-Pb collisions at $\sqrt{s_{NN}} = 2.76$ TeV", *JHEP* **05** (2016) 179,
       `arXiv:1506.08804 [nucl-ex]`.

[112] K. Zhou, N. Xu, Z. Xu, and P. Zhuang, "Medium effects on charmonium production at
       ultrarelativistic energies available at the CERN Large Hadron Collider",
       Phys. Rev. **C89** no. 5, (2014) 054911, `arXiv:1401.5845 [nucl-th]`.

[113] X. Du and R. Rapp, "Sequential regeneration of charmonia in heavy-ion collisions",
       Nucl. Phys. **A943** (2015) 147–158, `arXiv:1504.00670 [hep-ph]`.

[114] M. He, R. J. Fries, and R. Rapp, "Heavy-quark diffusion and hadronization in quark-gluon
       plasma", *Phys. Rev.* **C86** (2012) 014903, `arXiv:1106.6006 [nucl-th]`.

[115] S. Cao, K. J. Sun, S. Q. Li, S. Y. F. Liu, W. J. Xing, G. Y. Qin, and C. M. Ko, "Charmed hadron
       chemistry in relativistic heavy-ion collisions", *Phys. Lett.* **B807** (2020) 135561,
       `arXiv:1911.00456 [nucl-th]`.

[116] M. Nahrgang, J. Aichelin, P. B. Gossiaux, and K. Werner, "Influence of hadronic bound states
       above T_c on heavy-quark observables in Pb + Pb collisions at at the CERN Large Hadron
       Collider", *Phys. Rev.* **C89** no. 1, (2014) 014905, `arXiv:1305.6544 [hep-ph]`.

[117] R. Katz, C. A. G. Prado, J. Noronha-Hostler, J. Noronha, and A. A. P. Suaide, "Sensitivity study
       with a D and B mesons modular simulation code of heavy flavor R_{AA} and azimuthal anisotropies
       based on beam energy, initial conditions, hadronization, and suppression mechanisms",

Phys. Rev. **C102** no. 2, (2020) 024906, `arXiv:1906.10768` `[nucl-th]`.

[118] A. Beraudo, A. De Pace, M. Monteno, M. Nardi, and F. Prino, "Heavy flavors in heavy-ion collisions: quenching, flow and correlations", *Eur. Phys. J. C* **75** no. 3, (2015) 121, `arXiv:1410.6082` `[hep-ph]`.

[119] A. Beraudo, A. De Pace, M. Monteno, M. Nardi, and F. Prino, "Development of heavy-flavour flow-harmonics in high-energy nuclear collisions", *JHEP* **02** (2018) 043, `arXiv:1712.00588` `[hep-ph]`.

[120] S. Cao, T. Luo, G. Y. Qin, and X. N. Wang, "Linearized Boltzmann transport model for jet propagation in the quark-gluon plasma: heavy quark evolution", *Phys. Rev.* **C94** no. 1, (2016) 014909, `arXiv:1605.06447` `[nucl-th]`.

[121] S. Cao, T. Luo, G. Y. Qin, and X. N. Wang, "Heavy and light flavor jet quenching at RHIC and LHC energies", *Phys. Lett.* **B777** (2018) 255–259, `arXiv:1703.00822` `[nucl-th]`.

[122] S. Li and J. Liao, "Data-driven extraction of heavy quark diffusion in quark-gluon plasma", *Eur. Phys. J. C* **80** no. 7, (2020) 671, `arXiv:1912.08965` `[hep-ph]`.

[123] F. Scardina, S. K. Das, V. Minissale, S. Plumari, and V. Greco, "Estimating the charm quark diffusion coefficient and thermalization time from D meson spectra at energies available at the BNL Relativistic Heavy Ion Collider and the CERN Large Hadron Collider", *Phys. Rev.* **C96** no. 4, (2017) 044905, `arXiv:1707.05452` `[nucl-th]`.

[124] S. Plumari, G. Coci, V. Minissale, S. K. Das, Y. Sun, and V. Greco, "Heavy-light flavor correlations of anisotropic flows at LHC energies within event-by-event transport approach", *Phys. Lett.* **B805** (2020) 135460, `arXiv:1912.09350` `[hep-ph]`.

[125] W. Ke, Y. Xu, and S. A. Bass, "Modified Boltzmann approach for modeling the splitting vertices induced by the hot QCD medium in the deep Landau-Pomeranchuk-Migdal region", *Phys. Rev.* **C100** no. 6, (2019) 064911, `arXiv:1810.08177` `[nucl-th]`.

[126] T. Song, H. Berrehrah, D. Cabrera, J. M. Torres-Rincon, L. Tolos, W. Cassing, and E. Bratkovskaya, "Tomography of the quark-gluon-plasma by charm quarks", *Phys. Rev.* **C92** no. 1, (2015) 014910, `arXiv:1503.03039` `[nucl-th]`.

[127] **ALICE** Collaboration, S. Acharya *et al.*, "*D*-meson azimuthal anisotropy in mid-central Pb-Pb collisions at $\sqrt{s_{NN}} = $ **5.02** TeV", *Phys. Rev. Lett.* **120** no. 10, (2018) 102301, `arXiv:1707.01005` `[nucl-ex]`.

[128] C. B. Dover, U. Heinz, E. Schnedermann, and J. Zimányi, "Covariant coalescence model for relativistically expanding systems", *Phys. Rev.* **C44** (1991) 1636–1654.

[129] L. Ravagli and R. Rapp, "Quark coalescence based on a transport equation", *Phys. Lett.* **B655** (2007) 126–131, `arXiv:0705.0021` `[hep-ph]`.

[130] O. Kaczmarek, "Continuum estimate of the heavy quark momentum diffusion coefficient κ", *Nucl. Phys.* **A931** (2014) 633–637, `arXiv:1409.3724` `[hep-lat]`.

[131] H. T. Ding, A. Francis, O. Kaczmarek, F. Karsch, H. Satz, and W. Soeldner, "Charmonium properties in hot quenched lattice QCD", *Phys. Rev.* **D86** (2012) 014509, `arXiv:1204.4945` `[hep-lat]`.

[132] D. Banerjee, S. Datta, R. Gavai, and P. Majumdar, "Heavy quark momentum diffusion coefficient from lattice QCD", *Phys. Rev.* **D85** (2012) 014510, `arXiv:1109.5738` `[hep-lat]`.

[133] **STAR** Collaboration, L. Adamczyk *et al.*, "Measurement of D^0 azimuthal anisotropy at midrapidity in Au+Au collisions at $\sqrt{s_{NN}}$=200 GeV", *Phys. Rev. Lett.* **118** no. 21, (2017) 212301, `arXiv:1701.06060` `[nucl-ex]`.

[134] **PHENIX** Collaboration, A. Adare *et al.*, "Heavy quark production in $p + p$ and energy loss and flow of heavy quarks in Au+Au collisions at $\sqrt{s_{NN}} = 200$ GeV", *Phys. Rev.* **C84** (2011) 044905, `arXiv:1005.1627` `[nucl-ex]`.

[135] S. Cao *et al.*, "Toward the determination of heavy-quark transport coefficients in quark-gluon plasma", *Phys. Rev.* **C99** no. 5, (2019) 054907, `arXiv:1809.07894 [nucl-th]`.

[136] C. Loizides and A. Morsch, "Absence of jet quenching in peripheral nucleus–nucleus collisions", *Phys. Lett.* **B773** (2017) 408–411, `arXiv:1705.08856 [nucl-ex]`.

[137] **ALICE** Collaboration, S. Acharya *et al.*, "Analysis of the apparent nuclear modification in peripheral Pb–Pb collisions at 5.02 TeV", *Phys. Lett.* **B793** (2019) 420–432, `arXiv:1805.05212 [nucl-ex]`.

[138] **ALICE** Collaboration, S. Acharya *et al.*, "*D*-meson azimuthal anisotropy in midcentral Pb-Pb collisions at $\sqrt{s_{NN}} = 5.02$ TeV", *Phys. Rev. Lett.* **120** no. 10, (2018) 102301, `arXiv:1707.01005 [nucl-ex]`.

A   The ALICE Collaboration

S. Acharya[142], D. Adamová[97], A. Adler[75], J. Adolfsson[82], G. Aglieri Rinella[34], M. Agnello[30],
N. Agrawal[54], Z. Ahammed[142], S. Ahmad[16], S.U. Ahn[77], I. Ahuja[38], Z. Akbar[51], A. Akindinov[94],
M. Al-Turany[109], S.N. Alam[16], D. Aleksandrov[90], B. Alessandro[60], H.M. Alfanda[7], R. Alfaro Molina[72],
B. Ali[16], Y. Ali[14], A. Alici[25], N. Alizadehvandchali[126], A. Alkin[34], J. Alme[21], T. Alt[69], I. Altsybeev[114],
M.N. Anaam[7], C. Andrei[48], D. Andreou[92], A. Andronic[145], M. Angeletti[34], V. Anguelov[106],
F. Antinori[57], P. Antonioli[54], C. Anuj[16], N. Apadula[81], L. Aphecetche[116], H. Appelshäuser[69],
S. Arcelli[25], R. Arnaldi[60], I.C. Arsene[20], M. Arslandok[147], A. Augustinus[34], R. Averbeck[109], S. Aziz[79],
M.D. Azmi[16], A. Badalà[56], Y.W. Baek[41], X. Bai[130,109], R. Bailhache[69], Y. Bailung[50], R. Bala[103],
A. Balbino[30], A. Baldisseri[139], B. Balis[2], D. Banerjee[4], R. Barbera[26], L. Barioglio[107], M. Barlou[86],
G.G. Barnaföldi[146], L.S. Barnby[96], V. Barret[136], C. Bartels[129], K. Barth[34], E. Bartsch[69], F. Baruffaldi[27],
N. Bastid[136], S. Basu[82], G. Batigne[116], B. Batyunya[76], D. Bauri[49], J.L. Bazo Alba[113], I.G. Bearden[91],
C. Beattie[147], P. Becht[109], I. Belikov[138], A.D.C. Bell Hechavarria[145], F. Bellini[25], R. Bellwied[126],
S. Belokurova[114], V. Belyaev[95], G. Bencedi[146,70], S. Beole[24], A. Bercuci[48], Y. Berdnikov[100],
A. Berdnikova[106], L. Bergmann[106], M.G. Besoiu[68], L. Betev[34], P.P. Bhaduri[142], A. Bhasin[103],
I.R. Bhat[103], M.A. Bhat[4], B. Bhattacharjee[42], P. Bhattacharya[22], L. Bianchi[24], N. Bianchi[52],
J. Bielčík[37], J. Bielčíková[97], J. Biernat[119], A. Bilandzic[107], G. Biro[146], S. Biswas[4], J.T. Blair[120],
D. Blau[90,83], M.B. Blidaru[109], C. Blume[69], G. Boca[28,58], F. Bock[98], A. Bogdanov[95], S. Boi[22], J. Bok[62],
L. Boldizsár[146], A. Bolozdynya[95], M. Bombara[38], P.M. Bond[34], G. Bonomi[141,58], H. Borel[139],
A. Borissov[83], H. Bossi[147], E. Botta[24], L. Bratrud[69], P. Braun-Munzinger[109], M. Bregant[122], M. Broz[37],
G.E. Bruno[108,33], M.D. Buckland[129], D. Budnikov[110], H. Buesching[69], S. Bufalino[30], O. Bugnon[116],
P. Buhler[115], Z. Buthelezi[73,133], J.B. Butt[14], A. Bylinkin[128], S.A. Bysiak[119], M. Cai[27,7], H. Caines[147],
A. Caliva[109], E. Calvo Villar[113], J.M.M. Camacho[121], R.S. Camacho[45], P. Camerini[23],
F.D.M. Canedo[122], F. Carnesecchi[34,25], R. Caron[139], J. Castillo Castellanos[139], E.A.R. Casula[22],
F. Catalano[30], C. Ceballos Sanchez[76], P. Chakraborty[49], S. Chandra[142], S. Chapeland[34], M. Chartier[129],
S. Chattopadhyay[142], S. Chattopadhyay[111], A. Chauvin[22], T.G. Chavez[45], T. Cheng[7], C. Cheshkov[137],
B. Cheynis[137], V. Chibante Barroso[34], D.D. Chinellato[123], S. Cho[62], P. Chochula[34], P. Christakoglou[92],
C.H. Christensen[91], P. Christiansen[82], T. Chujo[135], C. Cicalo[55], L. Cifarelli[25], F. Cindolo[54],
M.R. Ciupek[109], G. Clai[II,54], J. Cleymans[I,125], F. Colamaria[53], J.S. Colburn[112], D. Colella[53,108,33],
A. Collu[81], M. Colocci[34], M. Concas[III,60], G. Conesa Balbastre[80], Z. Conesa del Valle[79], G. Contin[23],
J.G. Contreras[37], M.L. Coquet[139], T.M. Cormier[98], P. Cortese[31], M.R. Cosentino[124], F. Costa[34],
S. Costanza[28,58], P. Crochet[136], R. Cruz-Torres[81], E. Cuautle[70], P. Cui[7], L. Cunqueiro[98], A. Dainese[57],
M.C. Danisch[106], A. Danu[68], P. Das[88], P. Das[4], S. Das[4], S. Dash[49], A. De Caro[29], G. de Cataldo[53],
L. De Cilladi[24], J. de Cuveland[39], A. De Falco[22], D. De Gruttola[29], N. De Marco[60], C. De Martin[23],
S. De Pasquale[29], S. Deb[50], H.F. Degenhardt[122], K.R. Deja[143], L. Dello Stritto[29], W. Deng[7],
P. Dhankher[19], D. Di Bari[33], A. Di Mauro[34], R.A. Diaz[8], T. Dietel[125], Y. Ding[137,7], R. Divià[34],
D.U. Dixit[19], Ø. Djuvsland[21], U. Dmitrieva[64], J. Do[62], A. Dobrin[68], B. Dönigus[69], A.K. Dubey[142],
A. Dubla[109,92], S. Dudi[102], M. Dukhishyam[88], P. Dupieux[136], N. Dzalaiova[13], T.M. Eder[145],
R.J. Ehlers[98], V.N. Eikeland[21], F. Eisenhut[69], D. Elia[53], B. Erazmus[116], F. Ercolessi[25], F. Erhardt[101],
A. Erokhin[114], M.R. Ersdal[21], B. Espagnon[79], G. Eulisse[34], D. Evans[112], S. Evdokimov[93],
L. Fabbietti[107], M. Faggin[27], J. Faivre[80], F. Fan[7], A. Fantoni[52], M. Fasel[98], P. Fecchio[30], A. Feliciello[60],
G. Feofilov[114], A. Fernández Téllez[45], A. Ferrero[139], A. Ferretti[24], V.J.G. Feuillard[106], J. Figiel[119],
S. Filchagin[110], D. Finogeev[64], F.M. Fionda[55,21], G. Fiorenza[34,108], F. Flor[126], A.N. Flores[120],
S. Foertsch[73], S. Fokin[90], E. Fragiacomo[61], E. Frajna[146], U. Fuchs[34], N. Funicello[29], C. Furget[80],
A. Furs[64], J.J. Gaardhøje[91], M. Gagliardi[24], A.M. Gago[113], A. Gal[138], C.D. Galvan[121], P. Ganoti[86],
C. Garabatos[109], J.R.A. Garcia[45], E. Garcia-Solis[10], K. Garg[116], C. Gargiulo[34], A. Garibli[89],
K. Garner[145], P. Gasik[109], E.F. Gauger[120], A. Gautam[128], M.B. Gay Ducati[71], M. Germain[116],
P. Ghosh[142], S.K. Ghosh[4], M. Giacalone[25], P. Gianotti[52], P. Giubellino[109,60], P. Giubilato[27],
A.M.C. Glaenzer[139], P. Glässel[106], D.J.Q. Goh[84], V. Gonzalez[144], L.H. González-Trueba[72],

S. Gorbunov[39], M. Gorgon[2], L. Görlich[119], S. Gotovac[35], V. Grabski[72], L.K. Graczykowski[143], L. Greiner[81], A. Grelli[63], C. Grigoras[34], V. Grigoriev[95], S. Grigoryan[76,1], F. Grosa[34,60], J.F. Grosse-Oetringhaus[34], R. Grosso[109], G.G. Guardiano[123], R. Guernane[80], M. Guilbaud[116], K. Gulbrandsen[91], T. Gunji[134], W. Guo[7], A. Gupta[103], R. Gupta[103], S.P. Guzman[45], L. Gyulai[146], M.K. Habib[109], C. Hadjidakis[79], H. Hamagaki[84], M. Hamid[7], R. Hannigan[120], M.R. Haque[143], A. Harlenderova[109], J.W. Harris[147], A. Harton[10], J.A. Hasenbichler[34], H. Hassan[98], D. Hatzifotiadou[54], P. Hauer[43], L.B. Havener[147], S.T. Heckel[107], E. Hellbär[109], H. Helstrup[36], T. Herman[37], E.G. Hernandez[45], G. Herrera Corral[9], F. Herrmann[145], K.F. Hetland[36], H. Hillemanns[34], C. Hills[129], B. Hippolyte[138], B. Hofman[63], B. Hohlweger[92], J. Honermann[145], G.H. Hong[148], D. Horak[37], S. Hornung[109], A. Horzyk[2], R. Hosokawa[15], Y. Hou[7], P. Hristov[34], C. Hughes[132], P. Huhn[69], L.M. Huhta[127], C.V. Hulse[79], T.J. Humanic[99], H. Hushnud[111], L.A. Husova[145], A. Hutson[126], J.P. Iddon[34,129], R. Ilkaev[110], H. Ilyas[14], M. Inaba[135], G.M. Innocenti[34], M. Ippolitov[90], A. Isakov[97], T. Isidori[128], M.S. Islam[111], M. Ivanov[109], V. Ivanov[100], V. Izucheev[93], M. Jablonski[2], B. Jacak[81], N. Jacazio[34], P.M. Jacobs[81], S. Jadlovska[118], J. Jadlovsky[118], S. Jaelani[63], C. Jahnke[123,122], M.J. Jakubowska[143], A. Jalotra[103], M.A. Janik[143], T. Janson[75], M. Jercic[101], O. Jevons[112], A.A.P. Jimenez[70], F. Jonas[98,145], P.G. Jones[112], J.M. Jowett[34,109], J. Jung[69], M. Jung[69], A. Junique[34], A. Jusko[112], J. Kaewjai[117], P. Kalinak[65], A.S. Kalteyer[109], A. Kalweit[34], V. Kaplin[95], A. Karasu Uysal[78], D. Karatovic[101], O. Karavichev[64], T. Karavicheva[64], P. Karczmarczyk[143], E. Karpechev[64], V. Kashyap[88], A. Kazantsev[90], U. Kebschull[75], R. Keidel[47], D.L.D. Keijdener[63], M. Keil[34], B. Ketzer[43], Z. Khabanova[92], A.M. Khan[7], S. Khan[16], A. Khanzadeev[100], Y. Kharlov[93,83], A. Khatun[16], A. Khuntia[119], B. Kileng[36], B. Kim[17,62], C. Kim[17], D.J. Kim[127], E.J. Kim[74], J. Kim[148], J.S. Kim[41], J. Kim[106], J. Kim[74], M. Kim[106], S. Kim[18], T. Kim[148], S. Kirsch[69], I. Kisel[39], S. Kiselev[94], A. Kisiel[143], J.P. Kitowski[2], J.L. Klay[6], J. Klein[34], S. Klein[81], C. Klein-Bösing[145], M. Kleiner[69], T. Klemenz[107], A. Kluge[34], A.G. Knospe[126], C. Kobdaj[117], M.K. Köhler[106], T. Kollegger[109], A. Kondratyev[76], N. Kondratyeva[95], E. Kondratyuk[93], J. König[69], S.A. Konigstorfer[107], P.J. Konopka[34], G. Kornakov[143], S.D. Koryciak[2], A. Kotliarov[97], O. Kovalenko[87], V. Kovalenko[114], M. Kowalski[119], I. Králik[65], A. Kravčáková[38], L. Kreis[109], M. Krivda[112,65], F. Krizek[97], K. Krizkova Gajdosova[37], M. Kroesen[106], M. Krüger[69], E. Kryshen[100], M. Krzewicki[39], V. Kučera[34], C. Kuhn[138], P.G. Kuijer[92], T. Kumaoka[135], D. Kumar[142], L. Kumar[102], N. Kumar[102], S. Kundu[34], P. Kurashvili[87], A. Kurepin[64], A.B. Kurepin[64], A. Kuryakin[110], S. Kushpil[97], J. Kvapil[112], M.J. Kweon[62], J.Y. Kwon[62], Y. Kwon[148], S.L. La Pointe[39], P. La Rocca[26], Y.S. Lai[81], A. Lakrathok[117], M. Lamanna[34], R. Langoy[131], K. Lapidus[34], P. Larionov[34,52], E. Laudi[34], L. Lautner[34,107], R. Lavicka[115,37], T. Lazareva[114], R. Lea[141,23,58], J. Lehrbach[39], R.C. Lemmon[96], I. León Monzón[121], E.D. Lesser[19], M. Lettrich[34,107], P. Lévai[146], X. Li[11], X.L. Li[7], J. Lien[131], R. Lietava[112], B. Lim[17], S.H. Lim[17], V. Lindenstruth[39], A. Lindner[48], C. Lippmann[109], A. Liu[19], D.H. Liu[7], J. Liu[129], I.M. Lofnes[21], V. Loginov[95], C. Loizides[98], P. Loncar[35], J.A. Lopez[106], X. Lopez[136], E. López Torres[8], J.R. Luhder[145], M. Lunardon[27], G. Luparello[61], Y.G. Ma[40], A. Maevskaya[64], M. Mager[34], T. Mahmoud[43], A. Maire[138], M. Malaev[100], N.M. Malik[103], Q.W. Malik[20], S.K. Malik[103], L. Malinina[IV,76], D. Mal'Kevich[94], N. Mallick[50], G. Mandaglio[32,56], V. Manko[90], F. Manso[136], V. Manzari[53], Y. Mao[7], G.V. Margagliotti[23], A. Margotti[54], A. Marín[109], C. Markert[120], M. Marquard[69], N.A. Martin[106], P. Martinengo[34], J.L. Martinez[126], M.I. Martínez[45], G. Martínez García[116], S. Masciocchi[109], M. Masera[24], A. Masoni[55], L. Massacrier[79], A. Mastroserio[140,53], A.M. Mathis[107], O. Matonoha[82], P.F.T. Matuoka[122], A. Matyja[119], C. Mayer[119], A.L. Mazuecos[34], F. Mazzaschi[24], M. Mazzilli[34], M.A. Mazzoni[I,59], J.E. Mdhluli[133], A.F. Mechler[69], Y. Melikyan[64], A. Menchaca-Rocha[72], E. Meninno[115,29], A.S. Menon[126], M. Meres[13], S. Mhlanga[125,73], Y. Miake[135], L. Micheletti[60], L.C. Migliorin[137], D.L. Mihaylov[107], K. Mikhaylov[76,94], A.N. Mishra[146], D. Miśkowiec[109], A. Modak[4], A.P. Mohanty[63], B. Mohanty[88], M. Mohisin Khan[V,16], M.A. Molander[44], Z. Moravcova[91], C. Mordasini[107], D.A. Moreira De Godoy[145], I. Morozov[64], A. Morsch[34], T. Mrnjavac[34], V. Muccifora[52], E. Mudnic[35], D. Mühlheim[145], S. Muhuri[142], J.D. Mulligan[81], A. Mulliri[22], M.G. Munhoz[122], R.H. Munzer[69], H. Murakami[134], S. Murray[125], L. Musa[34], J. Musinsky[65], J.W. Myrcha[143], B. Naik[133,49], R. Nair[87], B.K. Nandi[49], R. Nania[54], E. Nappi[53],

A.F. Nassirpour[82], A. Nath[106], C. Nattrass[132], A. Neagu[20], L. Nellen[70], S.V. Nesbo[36], G. Neskovic[39], D. Nesterov[114], B.S. Nielsen[91], S. Nikolaev[90], S. Nikulin[90], V. Nikulin[100], F. Noferini[54], S. Noh[12], P. Nomokonov[76], J. Norman[129], N. Novitzky[135], P. Nowakowski[143], A. Nyanin[90], J. Nystrand[21], M. Ogino[84], A. Ohlson[82], V.A. Okorokov[95], J. Oleniacz[143], A.C. Oliveira Da Silva[132], M.H. Oliver[147], A. Onnerstad[127], C. Oppedisano[60], A. Ortiz Velasquez[70], T. Osako[46], A. Oskarsson[82], J. Otwinowski[119], M. Oya[46], K. Oyama[84], Y. Pachmayer[106], S. Padhan[49], D. Pagano[141,58], G. Paić[70], A. Palasciano[53], J. Pan[144], S. Panebianco[139], J. Park[62], J.E. Parkkila[127], S.P. Pathak[126], R.N. Patra[103,34], B. Paul[22], H. Pei[7], T. Peitzmann[63], X. Peng[7], L.G. Pereira[71], H. Pereira Da Costa[139], D. Peresunko[90,83], G.M. Perez[8], S. Perrin[139], Y. Pestov[5], V. Petráček[37], M. Petrovici[48], R.P. Pezzi[116,71], S. Piano[61], M. Pikna[13], P. Pillot[116], O. Pinazza[54,34], L. Pinsky[126], C. Pinto[26], S. Pisano[52], M. Płoskoń[81], M. Planinic[101], F. Pliquett[69], M.G. Poghosyan[98], B. Polichtchouk[93], S. Politano[30], N. Poljak[101], A. Pop[48], S. Porteboeuf-Houssais[136], J. Porter[81], V. Pozdniakov[76], S.K. Prasad[4], R. Preghenella[54], F. Prino[60], C.A. Pruneau[144], I. Pshenichnov[64], M. Puccio[34], S. Qiu[92], L. Quaglia[24], R.E. Quishpe[126], S. Ragoni[112], A. Rakotozafindrabe[139], L. Ramello[31], F. Rami[138], S.A.R. Ramirez[45], A.G.T. Ramos[33], T.A. Rancien[80], R. Raniwala[104], S. Raniwala[104], S.S. Räsänen[44], R. Rath[50], I. Ravasenga[92], K.F. Read[98,132], A.R. Redelbach[39], K. Redlich[VI,87], A. Rehman[21], P. Reichelt[69], F. Reidt[34], H.A. Reme-ness[36], Z. Rescakova[38], K. Reygers[106], A. Riabov[100], V. Riabov[100], T. Richert[82], M. Richter[20], W. Riegler[34], F. Riggi[26], C. Ristea[68], M. Rodríguez Cahuantzi[45], K. Røed[20], R. Rogalev[93], E. Rogochaya[76], T.S. Rogoschinski[69], D. Rohr[34], D. Röhrich[21], P.F. Rojas[45], P.S. Rokita[143], F. Ronchetti[52], A. Rosano[32,56], E.D. Rosas[70], A. Rossi[57], A. Roy[50], P. Roy[111], S. Roy[49], N. Rubini[25], O.V. Rueda[82], D. Ruggiano[143], R. Rui[23], B. Rumyantsev[76], P.G. Russek[2], R. Russo[92], A. Rustamov[89], E. Ryabinkin[90], Y. Ryabov[100], A. Rybicki[119], H. Rytkonen[127], W. Rzesa[143], O.A.M. Saarimaki[44], R. Sadek[116], S. Sadovsky[93], J. Saetre[21], K. Šafařík[37], S.K. Saha[142], S. Saha[88], B. Sahoo[49], P. Sahoo[49], R. Sahoo[50], S. Sahoo[66], D. Sahu[50], P.K. Sahu[66], J. Saini[142], S. Sakai[135], M.P. Salvan[109], S. Sambyal[103], V. Samsonov[I,100,95], D. Sarkar[144], N. Sarkar[142], P. Sarma[42], V.M. Sarti[107], M.H.P. Sas[147], J. Schambach[98], H.S. Scheid[69], C. Schiaua[48], R. Schicker[106], A. Schmah[106], C. Schmidt[109], H.R. Schmidt[105], M.O. Schmidt[34,106], M. Schmidt[105], N.V. Schmidt[98,69], A.R. Schmier[132], R. Schotter[138], J. Schukraft[34], K. Schwarz[109], K. Schweda[109], G. Scioli[25], E. Scomparin[60], J.E. Seger[15], Y. Sekiguchi[134], D. Sekihata[134], I. Selyuzhenkov[109,95], S. Senyukov[138], J.J. Seo[62], D. Serebryakov[64], L. Šerkšnytė[107], A. Sevcenco[68], T.J. Shaba[73], A. Shabanov[64], A. Shabetai[116], R. Shahoyan[34], W. Shaikh[111], A. Shangaraev[93], A. Sharma[102], H. Sharma[119], M. Sharma[103], N. Sharma[102], S. Sharma[103], U. Sharma[103], O. Sheibani[126], K. Shigaki[46], M. Shimomura[85], S. Shirinkin[94], Q. Shou[40], Y. Sibiriak[90], S. Siddhanta[55], T. Siemiarczuk[87], T.F. Silva[122], D. Silvermyr[82], T. Simantathammakul[117], G. Simonetti[34], B. Singh[107], R. Singh[88], R. Singh[103], R. Singh[50], V.K. Singh[142], V. Singhal[142], T. Sinha[111], B. Sitar[13], M. Sitta[31], T.B. Skaali[20], G. Skorodumovs[106], M. Slupecki[44], N. Smirnov[147], R.J.M. Snellings[63], C. Soncco[113], J. Song[126], A. Songmoolnak[117], F. Soramel[27], S. Sorensen[132], I. Sputowska[119], J. Stachel[106], I. Stan[68], P.J. Steffanic[132], S.F. Stiefelmaier[106], D. Stocco[116], I. Storehaug[20], M.M. Storetvedt[36], P. Stratmann[145], C.P. Stylianidis[92], A.A.P. Suaide[122], C. Suire[79], M. Sukhanov[64], M. Suljic[34], R. Sultanov[94], V. Sumberia[103], S. Sumowidagdo[51], S. Swain[66], A. Szabo[13], I. Szarka[13], U. Tabassam[14], S.F. Taghavi[107], G. Taillepied[136], J. Takahashi[123], G.J. Tambave[21], S. Tang[136,7], Z. Tang[130], J.D. Tapia Takaki[VII,128], M. Tarhini[116], M.G. Tarzila[48], A. Tauro[34], G. Tejeda Muñoz[45], A. Telesca[34], L. Terlizzi[24], C. Terrevoli[126], G. Tersimonov[3], S. Thakur[142], D. Thomas[120], R. Tieulent[137], A. Tikhonov[64], A.R. Timmins[126], M. Tkacik[118], A. Toia[69], N. Topilskaya[64], M. Toppi[52], F. Torales-Acosta[19], T. Tork[79], S.R. Torres[37], A. Trifiró[32,56], S. Tripathy[54,70], T. Tripathy[49], S. Trogolo[34,27], V. Trubnikov[3], W.H. Trzaska[127], T.P. Trzcinski[143], A. Tumkin[110], R. Turrisi[57], T.S. Tveter[20], K. Ullaland[21], A. Uras[137], M. Urioni[58,141], G.L. Usai[22], M. Vala[38], N. Valle[28,58], S. Vallero[60], L.V.R. van Doremalen[63], M. van Leeuwen[92], P. Vande Vyvre[34], D. Varga[146], Z. Varga[146], M. Varga-Kofarago[146], M. Vasileiou[86], A. Vasiliev[90], O. Vázquez Doce[52,107], V. Vechernin[114], E. Vercellin[24], S. Vergara Limón[45], L. Vermunt[63], R. Vértesi[146], M. Verweij[63], L. Vickovic[35], Z. Vilakazi[133], O. Villalobos Baillie[112],

G. Vino[53], A. Vinogradov[90], T. Virgili[29], V. Vislavicius[91], A. Vodopyanov[76], B. Volkel[34,106], M.A. Völkl[106], K. Voloshin[94], S.A. Voloshin[144], G. Volpe[33], B. von Haller[34], I. Vorobyev[107], D. Voscek[118], N. Vozniuk[64], J. Vrláková[38], B. Wagner[21], C. Wang[40], D. Wang[40], M. Weber[115], R.J.G.V. Weelden[92], A. Wegrzynek[34], S.C. Wenzel[34], J.P. Wessels[145], J. Wiechula[69], J. Wikne[20], G. Wilk[87], J. Wilkinson[109], G.A. Willems[145], B. Windelband[106], M. Winn[139], W.E. Witt[132], J.R. Wright[120], W. Wu[40], Y. Wu[130], R. Xu[7], A.K. Yadav[142], S. Yalcin[78], Y. Yamaguchi[46], K. Yamakawa[46], S. Yang[21], S. Yano[46], Z. Yin[7], I.-K. Yoo[17], J.H. Yoon[62], S. Yuan[21], A. Yuncu[106], V. Zaccolo[23], C. Zampolli[34], H.J.C. Zanoli[63], N. Zardoshti[34], A. Zarochentsev[114], P. Závada[67], N. Zaviyalov[110], M. Zhalov[100], B. Zhang[7], S. Zhang[40], X. Zhang[7], Y. Zhang[130], V. Zherebchevskii[114], Y. Zhi[11], N. Zhigareva[94], D. Zhou[7], Y. Zhou[91], J. Zhu[109,7], Y. Zhu[7], G. Zinovjev[3], N. Zurlo[141,58]

Affiliation Notes

[I] Deceased

[II] Also at: Italian National Agency for New Technologies, Energy and Sustainable Economic Development (ENEA), Bologna, Italy

[III] Also at: Dipartimento DET del Politecnico di Torino, Turin, Italy

[IV] Also at: M.V. Lomonosov Moscow State University, D.V. Skobeltsyn Institute of Nuclear, Physics, Moscow, Russia

[V] Also at: Department of Applied Physics, Aligarh Muslim University, Aligarh, India

[VI] Also at: Institute of Theoretical Physics, University of Wroclaw, Poland

[VII] Also at: University of Kansas, Lawrence, Kansas, United States

Collaboration Institutes

[1] A.I. Alikhanyan National Science Laboratory (Yerevan Physics Institute) Foundation, Yerevan, Armenia

[2] AGH University of Science and Technology, Cracow, Poland

[3] Bogolyubov Institute for Theoretical Physics, National Academy of Sciences of Ukraine, Kiev, Ukraine

[4] Bose Institute, Department of Physics and Centre for Astroparticle Physics and Space Science (CAPSS), Kolkata, India

[5] Budker Institute for Nuclear Physics, Novosibirsk, Russia

[6] California Polytechnic State University, San Luis Obispo, California, United States

[7] Central China Normal University, Wuhan, China

[8] Centro de Aplicaciones Tecnológicas y Desarrollo Nuclear (CEADEN), Havana, Cuba

[9] Centro de Investigación y de Estudios Avanzados (CINVESTAV), Mexico City and Mérida, Mexico

[10] Chicago State University, Chicago, Illinois, United States

[11] China Institute of Atomic Energy, Beijing, China

[12] Chungbuk National University, Cheongju, Republic of Korea

[13] Comenius University Bratislava, Faculty of Mathematics, Physics and Informatics, Bratislava, Slovakia

[14] COMSATS University Islamabad, Islamabad, Pakistan

[15] Creighton University, Omaha, Nebraska, United States

[16] Department of Physics, Aligarh Muslim University, Aligarh, India

[17] Department of Physics, Pusan National University, Pusan, Republic of Korea

[18] Department of Physics, Sejong University, Seoul, Republic of Korea

[19] Department of Physics, University of California, Berkeley, California, United States

[20] Department of Physics, University of Oslo, Oslo, Norway

[21] Department of Physics and Technology, University of Bergen, Bergen, Norway

[22] Dipartimento di Fisica dell'Università and Sezione INFN, Cagliari, Italy

[23] Dipartimento di Fisica dell'Università and Sezione INFN, Trieste, Italy

[24] Dipartimento di Fisica dell'Università and Sezione INFN, Turin, Italy

[25] Dipartimento di Fisica e Astronomia dell'Università and Sezione INFN, Bologna, Italy

[26] Dipartimento di Fisica e Astronomia dell'Università and Sezione INFN, Catania, Italy

[27] Dipartimento di Fisica e Astronomia dell'Università and Sezione INFN, Padova, Italy

[28] Dipartimento di Fisica e Nucleare e Teorica, Università di Pavia, Pavia, Italy

[29] Dipartimento di Fisica 'E.R. Caianiello' dell'Università and Gruppo Collegato INFN, Salerno, Italy

[30] Dipartimento DISAT del Politecnico and Sezione INFN, Turin, Italy

[31] Dipartimento di Scienze e Innovazione Tecnologica dell'Università del Piemonte Orientale and INFN Sezione di Torino, Alessandria, Italy

[32] Dipartimento di Scienze MIFT, Università di Messina, Messina, Italy

[33] Dipartimento Interateneo di Fisica 'M. Merlin' and Sezione INFN, Bari, Italy

[34] European Organization for Nuclear Research (CERN), Geneva, Switzerland

[35] Faculty of Electrical Engineering, Mechanical Engineering and Naval Architecture, University of Split, Split, Croatia

[36] Faculty of Engineering and Science, Western Norway University of Applied Sciences, Bergen, Norway

[37] Faculty of Nuclear Sciences and Physical Engineering, Czech Technical University in Prague, Prague, Czech Republic

[38] Faculty of Science, P.J. Šafárik University, Košice, Slovakia

[39] Frankfurt Institute for Advanced Studies, Johann Wolfgang Goethe-Universität Frankfurt, Frankfurt, Germany

[40] Fudan University, Shanghai, China

[41] Gangneung-Wonju National University, Gangneung, Republic of Korea

[42] Gauhati University, Department of Physics, Guwahati, India

[43] Helmholtz-Institut für Strahlen- und Kernphysik, Rheinische Friedrich-Wilhelms-Universität Bonn, Bonn, Germany

[44] Helsinki Institute of Physics (HIP), Helsinki, Finland

[45] High Energy Physics Group, Universidad Autónoma de Puebla, Puebla, Mexico

[46] Hiroshima University, Hiroshima, Japan

[47] Hochschule Worms, Zentrum für Technologietransfer und Telekommunikation (ZTT), Worms, Germany

[48] Horia Hulubei National Institute of Physics and Nuclear Engineering, Bucharest, Romania

[49] Indian Institute of Technology Bombay (IIT), Mumbai, India

[50] Indian Institute of Technology Indore, Indore, India

[51] Indonesian Institute of Sciences, Jakarta, Indonesia

[52] INFN, Laboratori Nazionali di Frascati, Frascati, Italy

[53] INFN, Sezione di Bari, Bari, Italy

[54] INFN, Sezione di Bologna, Bologna, Italy

[55] INFN, Sezione di Cagliari, Cagliari, Italy

[56] INFN, Sezione di Catania, Catania, Italy

[57] INFN, Sezione di Padova, Padova, Italy

[58] INFN, Sezione di Pavia, Pavia, Italy

[59] INFN, Sezione di Roma, Rome, Italy

[60] INFN, Sezione di Torino, Turin, Italy

[61] INFN, Sezione di Trieste, Trieste, Italy

[62] Inha University, Incheon, Republic of Korea

[63] Institute for Gravitational and Subatomic Physics (GRASP), Utrecht University/Nikhef, Utrecht, Netherlands

[64] Institute for Nuclear Research, Academy of Sciences, Moscow, Russia

[65] Institute of Experimental Physics, Slovak Academy of Sciences, Košice, Slovakia

[66] Institute of Physics, Homi Bhabha National Institute, Bhubaneswar, India

[67] Institute of Physics of the Czech Academy of Sciences, Prague, Czech Republic

[68] Institute of Space Science (ISS), Bucharest, Romania

[69] Institut für Kernphysik, Johann Wolfgang Goethe-Universität Frankfurt, Frankfurt, Germany

[70] Instituto de Ciencias Nucleares, Universidad Nacional Autónoma de México, Mexico City, Mexico

[71] Instituto de Física, Universidade Federal do Rio Grande do Sul (UFRGS), Porto Alegre, Brazil

[72] Instituto de Física, Universidad Nacional Autónoma de México, Mexico City, Mexico

[73] iThemba LABS, National Research Foundation, Somerset West, South Africa

[74] Jeonbuk National University, Jeonju, Republic of Korea

[75] Johann-Wolfgang-Goethe Universität Frankfurt Institut für Informatik, Fachbereich Informatik und Mathematik, Frankfurt, Germany

[76] Joint Institute for Nuclear Research (JINR), Dubna, Russia

[77] Korea Institute of Science and Technology Information, Daejeon, Republic of Korea

[78] KTO Karatay University, Konya, Turkey

[79] Laboratoire de Physique des 2 Infinis, Irène Joliot-Curie, Orsay, France

[80] Laboratoire de Physique Subatomique et de Cosmologie, Université Grenoble-Alpes, CNRS-IN2P3, Grenoble, France

[81] Lawrence Berkeley National Laboratory, Berkeley, California, United States

[82] Lund University Department of Physics, Division of Particle Physics, Lund, Sweden

[83] Moscow Institute for Physics and Technology, Moscow, Russia

[84] Nagasaki Institute of Applied Science, Nagasaki, Japan

[85] Nara Women's University (NWU), Nara, Japan

[86] National and Kapodistrian University of Athens, School of Science, Department of Physics , Athens, Greece

[87] National Centre for Nuclear Research, Warsaw, Poland

[88] National Institute of Science Education and Research, Homi Bhabha National Institute, Jatni, India

[89] National Nuclear Research Center, Baku, Azerbaijan

[90] National Research Centre Kurchatov Institute, Moscow, Russia

[91] Niels Bohr Institute, University of Copenhagen, Copenhagen, Denmark

[92] Nikhef, National institute for subatomic physics, Amsterdam, Netherlands

[93] NRC Kurchatov Institute IHEP, Protvino, Russia

[94] NRC «Kurchatov»Institute - ITEP, Moscow, Russia

[95] NRNU Moscow Engineering Physics Institute, Moscow, Russia

[96] Nuclear Physics Group, STFC Daresbury Laboratory, Daresbury, United Kingdom

[97] Nuclear Physics Institute of the Czech Academy of Sciences, Řež u Prahy, Czech Republic

[98] Oak Ridge National Laboratory, Oak Ridge, Tennessee, United States

[99] Ohio State University, Columbus, Ohio, United States

[100] Petersburg Nuclear Physics Institute, Gatchina, Russia

[101] Physics department, Faculty of science, University of Zagreb, Zagreb, Croatia

[102] Physics Department, Panjab University, Chandigarh, India

[103] Physics Department, University of Jammu, Jammu, India

[104] Physics Department, University of Rajasthan, Jaipur, India

[105] Physikalisches Institut, Eberhard-Karls-Universität Tübingen, Tübingen, Germany

[106] Physikalisches Institut, Ruprecht-Karls-Universität Heidelberg, Heidelberg, Germany

[107] Physik Department, Technische Universität München, Munich, Germany

[108] Politecnico di Bari and Sezione INFN, Bari, Italy

[109] Research Division and ExtreMe Matter Institute EMMI, GSI Helmholtzzentrum für Schwerionenforschung GmbH, Darmstadt, Germany

[110] Russian Federal Nuclear Center (VNIIEF), Sarov, Russia

[111] Saha Institute of Nuclear Physics, Homi Bhabha National Institute, Kolkata, India

[112] School of Physics and Astronomy, University of Birmingham, Birmingham, United Kingdom

[113] Sección Física, Departamento de Ciencias, Pontificia Universidad Católica del Perú, Lima, Peru

[114] St. Petersburg State University, St. Petersburg, Russia

[115] Stefan Meyer Institut für Subatomare Physik (SMI), Vienna, Austria

[116] SUBATECH, IMT Atlantique, Université de Nantes, CNRS-IN2P3, Nantes, France

[117] Suranaree University of Technology, Nakhon Ratchasima, Thailand

[118] Technical University of Košice, Košice, Slovakia

[119] The Henryk Niewodniczanski Institute of Nuclear Physics, Polish Academy of Sciences, Cracow, Poland

[120] The University of Texas at Austin, Austin, Texas, United States

[121] Universidad Autónoma de Sinaloa, Culiacán, Mexico

[122] Universidade de São Paulo (USP), São Paulo, Brazil

[123] Universidade Estadual de Campinas (UNICAMP), Campinas, Brazil

[124] Universidade Federal do ABC, Santo Andre, Brazil

[125] University of Cape Town, Cape Town, South Africa

[126] University of Houston, Houston, Texas, United States

[127] University of Jyväskylä, Jyväskylä, Finland

[128] University of Kansas, Lawrence, Kansas, United States

[129] University of Liverpool, Liverpool, United Kingdom

[130] University of Science and Technology of China, Hefei, China

[131] University of South-Eastern Norway, Tonsberg, Norway

[132] University of Tennessee, Knoxville, Tennessee, United States

[133] University of the Witwatersrand, Johannesburg, South Africa

[134] University of Tokyo, Tokyo, Japan

[135] University of Tsukuba, Tsukuba, Japan

[136] Université Clermont Auvergne, CNRS/IN2P3, LPC, Clermont-Ferrand, France

[137] Université de Lyon, CNRS/IN2P3, Institut de Physique des 2 Infinis de Lyon, Lyon, France

[138] Université de Strasbourg, CNRS, IPHC UMR 7178, F-67000 Strasbourg, France, Strasbourg, France

[139] Université Paris-Saclay Centre d'Etudes de Saclay (CEA), IRFU, Départment de Physique Nucléaire (DPhN), Saclay, France

[140] Università degli Studi di Foggia, Foggia, Italy

[141] Università di Brescia, Brescia, Italy

[142] Variable Energy Cyclotron Centre, Homi Bhabha National Institute, Kolkata, India

[143] Warsaw University of Technology, Warsaw, Poland

[144] Wayne State University, Detroit, Michigan, United States

[145] Westfälische Wilhelms-Universität Münster, Institut für Kernphysik, Münster, Germany

[146] Wigner Research Centre for Physics, Budapest, Hungary

[147] Yale University, New Haven, Connecticut, United States

[148] Yonsei University, Seoul, Republic of Korea